University of Utrecht

Faculty of Geosciences

Master Thesis

A multiproxy approach study of the inland Mississippi delta: paleoenvironment, marine transgression and subsidence during the Holocene and carbon burial potential

---

Josh Guyat

6876595

07/06/2022

Supervisors: dr. Francesca Sangiorgi, dr. Francien Peterse, Yord Yedema, dr. Timme Donders

Acknowledgements

I would like to thank the following people, without whom I would not have been able to complete this research project. Firstly to dr. Francesca Sangiorgi who found time and patience to offer her invaluable guidance and expertise to me, and the many other students in our study area. I would like to thank dr. Francien Peterse for her knowledge and guidance on organic geochemistry and lipid biomarkers. To a great surprise to me chemistry, a subject I previously struggled with in high school, is now something I aim to peruse in the future due to Francien's teaching and fascinating research. I would like to thank dr. Timme Donders for his extensive knowledge of pollen and help with identification. I would like to thank Yord Yedema for always being available, whether offering help during my lab work, for my data analyses and my writing style, he was always there to offer great advice and guidance. I would like to give special thanks to my supervisors as a whole, for finding time in their busy schedules to meet together and discuss my research. I am profoundly grateful for the Utrecht University lab technicians, their training and patience with students learning new techniques was invaluable. Lastly, I would like thank both my friends here in Utrecht and from the U.K. for offering advice and support during this research project.

Contents

1. Abstract

Wetland environments are disappearing at an alarming rate, driven through rising sea levels, a warming climate and human-driven subsidence, a consequent from engineering and damming the natural flow and cycle of river systems. In addition to housing a vast biodiversity, attenuating storm surges and holding a large economic value, wetlands also act as the largest carbon sink per hectare. The Mississippi Delta has long undergone severe land and wetland loss with 5000 km^2 of wetlands disappearing from the Louisiana coastlines. A multiproxy approach using bulk sediment, geochemical and palynological analyses has been conducted on a 38.7 m core taken during the installation of a subsidence monitoring superstation close to the Mississippi River, southeast of New Orleans. This new data, in addition to previous stratigraphic lithology description, has been used to interpret the depositional evolution of the Holocene Mississippi River Delta (MRD) and explore the carbon storage potential of the delta environment. An initial Holocene transgression between 38.7 and 28 m has been interpreted. Increased fluvial input into the coastal marine realm, but remaining within a pro delta environment between 27 and 19.5 m is inferred primarily through biomarkers. A lithology change between 19.5 and 9.5 m shows the transition from marine pro delta towards a more terrestrial environment with the deposition of a delta mouth bar. 9.5 to 2 m reflects a predominantly terrestrial environment. Here the influence of delta lobe switching on the depositional environment is clear with the St. Bernard, Lafouche and Plaquesmines-Modern sub-deltas redirecting and redistributing water and sediment across the Mississippi Delta landscape. Within the upper 2 m human influences such as damming the MRD are shown in the environment, reducing sediment load and therefore terrestrial signals to the study site. Two zones of optimal carbon storage have been identified, with the lithology, palynology, BIT Index and $F_{C32\ 1,15}$ inferring a wetland environment. Carbon storage potential is inferred through total organic carbon and the n-alkane carbon preference indicator. The data supports initial lithological interpretation of the MRD and highlights the need for the protection and restoration these wetland environments with high carbon storage potential.

2. Introduction

Coastal wetland and delta environments play an important role in the global carbon cycle whilst also providing essential ecological and economic services to the coastal communities they support. The importance of wetland landscapes within a coastal deltaic basin is further supported by their ability to reduce flood risk (Twilley et al., 2016) and therefore protect the large populations inhabiting them. Land loss and reduction of these wetlands therefore has significant economic and social impacts directly affecting both local and global communities.

Human engineering to minimise the risk of flooding on delta plains has reduced sediment supply, resulting in loss of land and consequently a negative feedback to sustain land area (Twilley et al., 2016). By removing the delta's ability to produce wetlands that attenuate storm surges, the damage of extreme weather events, such as Hurricane Katrina in 2005, has significantly increased. In addition, deltas and their wetlands are areas where the preservation and burial of terrestrial organic matter significantly contribute to the global carbon cycle. Terrestrial organic carbon derived from photosynthetically fixed CO_2, if buried in sediments, has a substantial influence over the CO_2/O_2 balance in the atmosphere (Zong et al., 2010). The high sedimentation rates of deltas over large areas allow them to collectively bury 75 Tg of organic carbon (OC) annually and therefore form a major link between short and long term carbon cycles (Shields et al., 2017). Blue carbon sinks, defined as the OC produced and buried in coastal ecosystems, are formed on coastal wetlands and sequester CO_2 at rates 50 times that of equal forested areas (McLeod et al., 2011). Sedimentation rate, burial efficiency and thus carbon sequestration change under different climates and delta environments. Despite a relatively small surface area, the coastal zone plays a considerable role in the biogeochemical cycles due to the large amounts of matter exchanged between the terrestrial and ocean realm.

Wetlands cover just 2% of the Earth's surface but store 20% of global organic ecosystem carbon. This disproportional share is driven by high carbon sequestration rates that are multitudes higher than terrestrial and oceanic ecosystems Temmink et al., (2022). Wetlands store the bulk of organic matter (OM) as soil organic matter with the highest carbon density of 1000 to 2000 Mg C ha^{-1} in peatlands, compared to 150 to 230 Mg C ha^{-1} in terrestrial forests (Emerson and Hedges, 1988; MacDicken et al., 2016). Tropical peatlands sequester internal and externally produced OC at a rate of 200g C m^{-2} $year^{-1}$ (McLeod et al., 2011). Within coastal ecosystems this can be amplified by external OC input from riverine and marine sources (Middelberg et al., 1997). The carbon storage capabilities of wetlands are controlled by two feedback mechanisms (Fig. 1). Wetlands driven by 'productivity-stimulating' feedbacks are driven by processes that increase resource availability stimulating vegetation growth and OM production. These ecosystems are often coastal, with external OM arriving into the ecosystem from fluvial and marine sources. With increased sediment input, the ecosystem can however become self-limiting as the system ages and grows, outpacing sea level rise (Temmink et al., 2022). Wetlands driven by 'decomposition-limiting' feedbacks are often primarily fed by

rainwater. When peat rises above groundwater, vegetation and their detrital remains limit lateral and vertical drainage. This results in continual waterlogged, nutrient-limited and anoxic conditions (Clymo et al., 1964) with slower production and therefore higher accumulation of OM (Temmink et al., 2022).

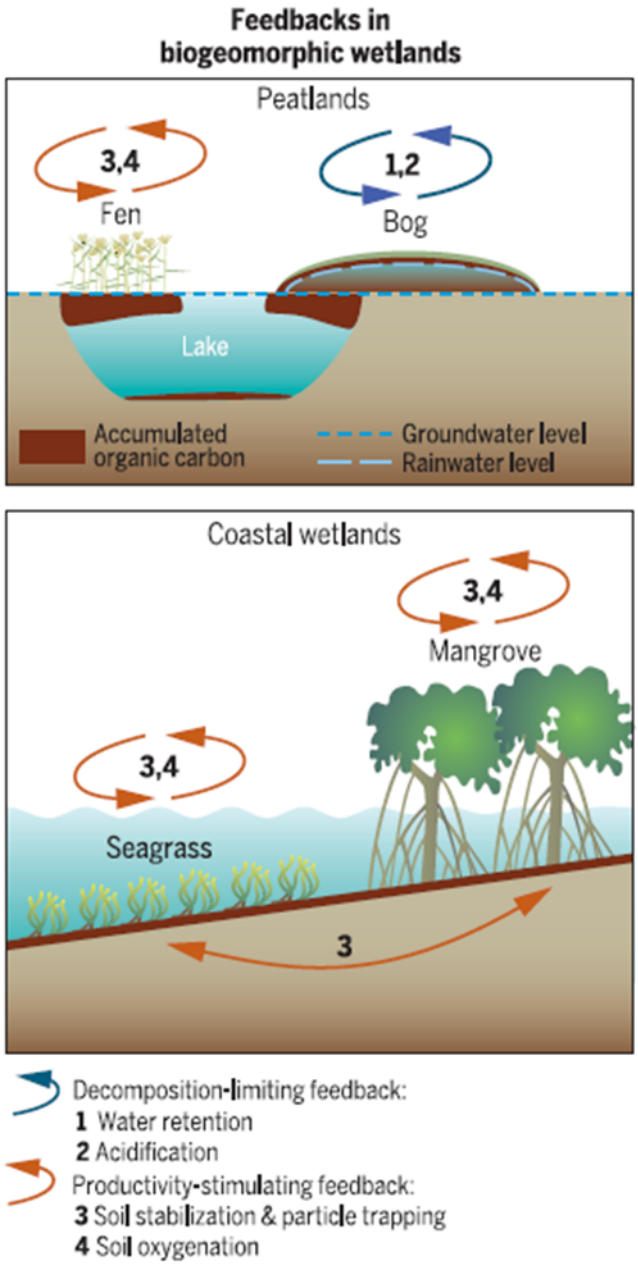

Figure 1. Feedback mechanisms in wetlands. A) Productivity-stimulating increases resource availability promoting vegetation growth. Decomposition-limited is stronger than productivity-stimulating in wetlands resulting in net accumulation of OM. In Fens, system starts as productivity-limited before rising above groundwater and becoming decomposition-limited. B) Coastal ecosystems generate productivity-stimulated feedback that trap external OM and enhance local production. From Temmink et al., (2022).

The present-day Mississippi River is a continental scale sediment dispersal system and the fourth largest drainage basin worldwide (Fig. 2), draining 3.4 x 10^6 km^2 (Syvitski and Milliman, 2007; Blum and Roberts, 2012). The trunk streams heads in Minnesota before flowing south

entering the Mississippi embayment, with the Ohio River tributary draining the Appalachians and eastern United States and the Missouri River draining the northern Rockies. The Ohio River provides most of the water and the Missouri River provides most of the sediment (Knox, 2007; Meade and Moody, 2010). Water and sediment is then transferred through the Lower Mississippi ~1000 km south where it has constructed the Holocene Mississippi Delta Plain that makes up most of Louisiana (Blum and Roberts, 2012). The coastal area of Louisiana is an important economic and environmental natural resource to the U.S. making up 40% of the wetlands in the continental U.S. (Couvillion and Beck, 2013). The modern delta region supports 30% of U.S. coastal fisheries (Day et al., 2017) and is a prolific hydrocarbon province, housing infrastructure for ~25% of US hydrocarbon production. Furthermore, with the south Louisiana port handing ~20% of US waterborne commerce (Blum and Roberts, 2012) the socio-economic benefits and reliance on the delta is evident. Previous attention to wetland loss by Fisk (1944) and Russell (1936) was largely ignored and now, less than a century later, >25% of deltaic wetlands have disappeared (Couvillion et al., 2011) with significant consequences to the environment and economic and societal stability of the populations that inhabit them.

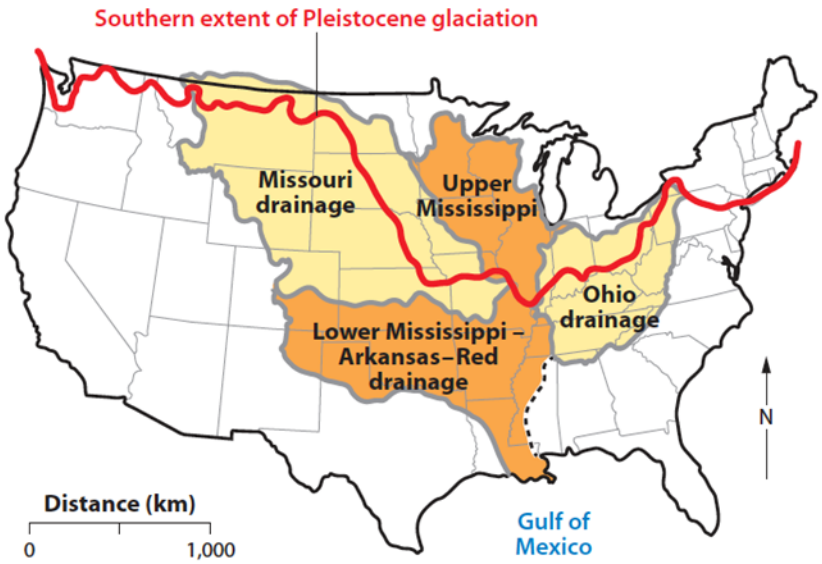

Figure 2. *The Mississippi drainage basin. Red - Maximum extent of Pleistocene ice sheets. Major tributary basins. From Blum and Roberts (2012)*

The Mississippi River Delta (MRD) has long undergone severe land and wetland loss and since the 1930s almost 5000 km^2 of wetlands have disappeared from the Louisiana coastlines (Couvillion and Beck, 2013). Subsidence, a natural phenomenon in the delta cycle, is exacerbated by the extraction of hydrocarbons and groundwater. Dam emplacement, land reclamation via drainage and the continued threat of sea level rise are driving changes of previously unseen scale producing landscape transformations new to geology and that cannot be explained by traditional models (Russell et al., 2021). The natural delta lobe switching events of deltas play an important role in the loss of land in Louisiana (Roberts, 1997).

Deltas are inherently dynamic and undergo cyclic lobe switching events 1000-1500 years (Bentely et al., 2014) when the river takes a new route to the sea, leaving the abandoned lobe starved of sediment and subject to erosion while subsiding under its own weight (Bentely et al., 2016). Lobe switching and the associated environments, and relation to the MRD, follow known trends and patterns (Fig. 3). Delta lobe switching can occur abruptly or gradually over centuries, by flood events that find a new, less resistant path to the coast (Bentely et al., 2014). Through delta lobe switching, the Mississippi Delta has distributed sediment along ~300 km of coastline (Coleman, 1988) with the rate of growth controlled by sediment supply. Within the Mississippi delta plain the river dynamics and energy levels are reflected in the sedimentary system. Sediment deposited in or close to the active river channel is coarser, sandy grained whereas sediment deposited further from the channel is often mud rich (Allen, 1965; Russell et al, 2021). In the Lower Mississippi River Valley, the floodplain can extent 100 km across, with the flood-prone area being >90,000 km^2 (Galloway, 2004). As flooding events occur over time, thin muddy layers can accumulate tens of km away from the river and build the surrounding landscape (Miall, 1985). In the Holocene the Mississippi River was free to meander across the floodplain and through this process the channel constantly changes course and remodelled the landscape through time (Russell et al., 2021). Most of the delta landscape consists of freshwater / brackish wetlands often featuring small lakes occurring between alluvial ridges and towards the coast (Blum and Roberts, 2021). When coastal marshes are formed in a deltaic progradation cycle it is referred to as the constructional phase (Scruton, 1960). After avulsion and abandonment of the major sediment deposition site, the environment is subject to marine reworking and subsidence, resulting in inundation of the marsh by saline waters and eventually transgressed by marine waters into a bay environment (Coleman and Roberts 1989). This has been referred to by Scruton (1960) as the destructional phase, and can occur over relatively short periods of time. During the last few decades, the natural cyclicity of deltas has however been heavily influenced and altered by human activities. To predict and plan for future coastal development, it is essential to understand the history of wetland development in the MRD in relation to internal and external drivers in the Holocene.

During recent decades, cyclic lobe switching (Coleman, 1999; Coleman et al., 1998; Yao et al., 2020), sea level (Nelson and Bray, 1970; Curray, 1961; Törnqvist et al., 2004) and subsidence (Morton and Bernier, 2010; Bridgeman, 2018) have been documented in the MRD region. It is generally accepted that six major delta complexes were developed since the mid-Holocene. The Sale-Cypremont (4600-3500 BP), Teche (~3500-2800 BP), St. Bernard (~2800-1000 BP), Lafourche (~1000-300 BP), Plaquemine-Balize (750 BP-present) and the Atchafalaya-Wax Lake (400 BP-Present) (Yao et al., 2020). The position of delta lobes, in relation to a study site, has a profound effect on ecosystem development through the mid-Holocene as shown by Yao et al., (2020) on the eastern end of Louisiana's Chenier Plain. Between 5190 and 4240 cal yr BP, during a time of slow relative SL rise, the study site was occupied by a swamp. The formation

of the Sale-Cypermont subdelta transformed the marsh environment to a maritime forest suggesting propagation of the shoreline. The Mississippi river delta lobe switched to a more easterly position, redistributing sediment away from the study site and forming the Teche, St. Bernard, Lafourche and Plaquemine-Balize complexes. This transformed the study site to a freshwater swamp between 3440 and 1250 cal yr BP and then to a coastal marsh between 1520 and 300 cal yr BP. From 300 cal yr BP the Atchafalya-Wax Lake sub-delta complex formed a modern-day beach coastal ecosystem. Yao et al., (2020) therefore shows how shoreline progradation can be controlled by internal processes of lobe switching and sediment supply and the effects it has on sustaining coastal wetlands in Louisiana.

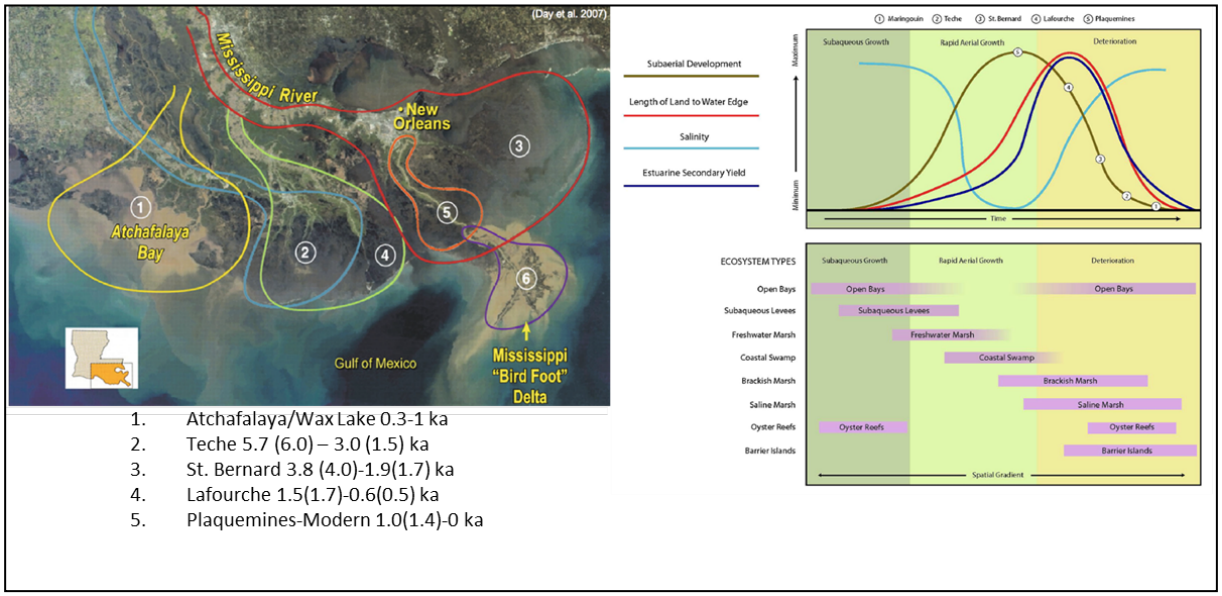

Figure 3. *Map of the Mississippi River Delta Plain (MRDP) based on satellite image overlaid with the historical delta lobe occurrences over the last 7000 years (from Day et al. 2007). Bottom: Ecosystem development along spatial and temporal gradient related to sediment delivery and distribution of ecosystem types in coastal basin. From Twilley et al., (2016) modified from (Gagliano and Van Beek 1975); (Gosselink et al., 1998). Numbers on the subaerial development line correspond to delta lobes above.*

Sea level rise accompanied deglaciation through the Late Pleistocene and Early Holocene, with rapid sea level rise associated with meltwater pulses occurring during the start of the Holocene (Bard et al., 1996). Global ice volumes and sea level approached present-day values by ~6 ka with little change since (Church et al., 2008). In the Mississippi Delta region, relative sea level (RSL) equals global mean sea level rise plus subsidence. As subsidence is a known natural phenomena of delta lobes, the internal processes of the delta plain have a significant effect on RSL. Overall, the RSL history of the GOM remains highly controversial, with a large variability of reconstructed patterns, ranging from 'stair-step' of short periods of rapid RSL rise with alternating stillstands (Frazier, 1974; Curray, 1961) and even RSL falls (Nelson and Bray, 1970). Törnqvist and Gonzalez., (2004), through an extensive sampling program using basal peats, found a RSL rise followed a relatively smooth trend between 8 – 3 ka (Fig. 4).

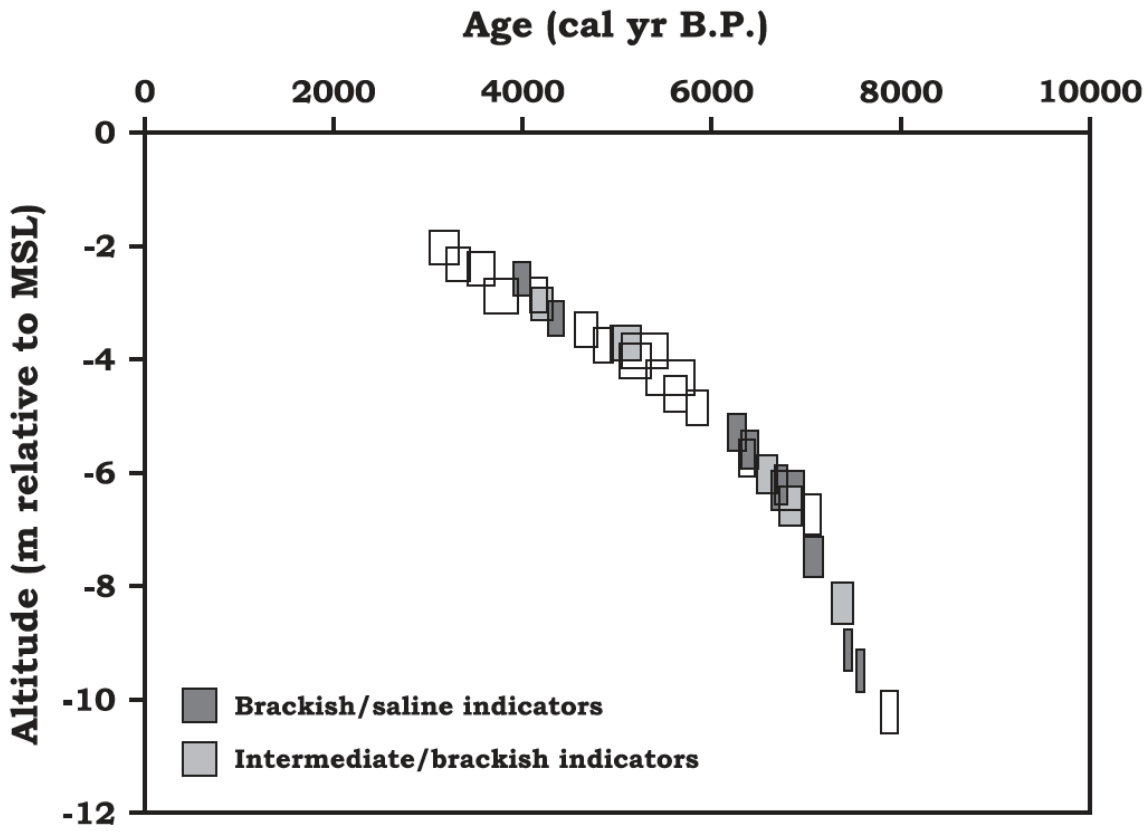

Figure 4. *RSL curve of the Lutcher-Gramercy area, eastern margin of the Mississippi Delta with 95% probability. Törnqvist et al., (2004).*

The underlying geology of the MRD ultimately affects the processes occurring today. The fluvial and shallow marine sediments are inherently unstable and prone to (Blum and Roberts, 2021; Galloway, 2008). The modern-day MRD morphology formed during the Quaternary, it is however important to understand the geological history of the MRD and the processes that drive the environmental and human influences seen today. Modern land surface dynamics are conditioned by the longer-term processes that started to act on the Mississippi depocenter during the Late Cretaceous (Blum and Roberts 2012, Cox and Van Arsdale 2003). Through the Cretaceous, large-scale processes such as the Laramide orogeny (80-55 Ma) (English and Johnston, 2004) and tectonic changes transformed the drainage patterns of the early Mississippi River reconfiguring drainage into the Gulf of Mexico by at least the Maastrichtian (72-66 Ma) (Potter-McIntyre et al., 2018). Between 60 – 30 Ma, the Palaeo-Mississippi River captured the drainage of other palaeo-rivers and grew in dominance. The sediment that this new river brought to the Gulf coast built 200 km of land southward into the marine realm and thus formed the foundation of the Mississippi Delta (Russel et al., 2021; Bentley et al., 2016).

During the Quaternary (2.6 Ma) in North America, the hydrodynamic landscape was dominated and controlled by the Laurentide ice sheet (Russell et al., 2021). Ice sheets exert control by periods of advance and retreat over the landscape. At the last glacial maximum

(LGM) land-bound ice held enough water to drop sea level by 130 m (Wickert et al., 2013) and, in the case of the Laurentide ice sheet, depress the crust in North America by 300 m (Fulton and Prest, 1987). As the Laurentide ice sheet waxed and waned over 50 times during the Quaternary, it intercepted, rerouted and permanently modified river systems contributing to the Mississippi (Russell et al., 2021). In response to Glacial/Interglacial cycles, the hydrological regime of the Mississippi River continually altered its morphology, reacting to variations in water and sediment supply (Blum and Törnqvist, 2000; Wickert et al., 2013). As the Laurentide ice sheet melted, the period between 15-12 ka BP saw the greatest loss of ice volume (Aharon, 2013), swelling the Mississippi River with glacial meltwater and coarser sediment, transforming the river into a multi-braided river system (Russell et al., 2021). The period of meltwater release and mega floods permanently changed the Mississippi drainage system, with the beginning of the Holocene seeing the change from a dominantly braided system to the present-day meandering river morphology (Rittenour et al., 2007). As global sea levels rose by roughly 120 m (Clark et al., 2016) between 17000 – 7500 years ago, the river delta continued to develop with later stabilisation of the landscape in a warming climate by Holocene grasslands and woodlands (Russell et al., 2021). Vertical displacement and average subsidence rates, calculated by Bridgeman (2018) via radiocarbon and OSL ages as far back as ~3.5 Ka show values as high as 8 m of vertical displacement. It is inferred that compaction of the thick, underlying muds of the pro delta and hydrocarbon and groundwater extraction are the drivers of these accelerated rates of subsidence.

In order to better understand the environmental changes of the Mississippi throughout the Holocene and further understand the role wetlands plays in carbon storage, a multi-proxy approach will be conducted on an existing core from the MRD. The field site is within the Plaquesmines–modern subdelta south of Belle Chasse Louisiana, located two km from the Mississippi River and 170 m from the Coastal Reference Monitoring (CRMS) site 0276 (Fig. 5). five km north is the Mid-Barataria sediment diversion, a primary target area to build new land in the MRD. Levees have cut the study area delta plain off from the Mississippi's direct water and sediment supply since as early as 1888, leaving a marsh environment with an accretion rate of 14.4 mm/yr (Bridgeman, 2018). The analysis and description of cores from the field site, Myrtle Grove I (henceforth 'MG') superstation is part of a larger interdisciplinary effort to study the depth and temporal variability of subsidence (Allison et al., 2016). At the superstation, a core of 37.8 m was collected in January 2016 by Fugro and taken to Tulane University for stratigraphic analysis. With a Pleistocene basal peat at the core base, it can be confidently assumed the core contains a record of the Holocene. Radiocarbon and OSL dating of charcoal and seeds and sand have allowed for the creation of an age depth plot. However, as constant accumulation rates between dated samples are assumed, and the relative lack of dated samples, the reliability of the age depth plot must be taken into account.

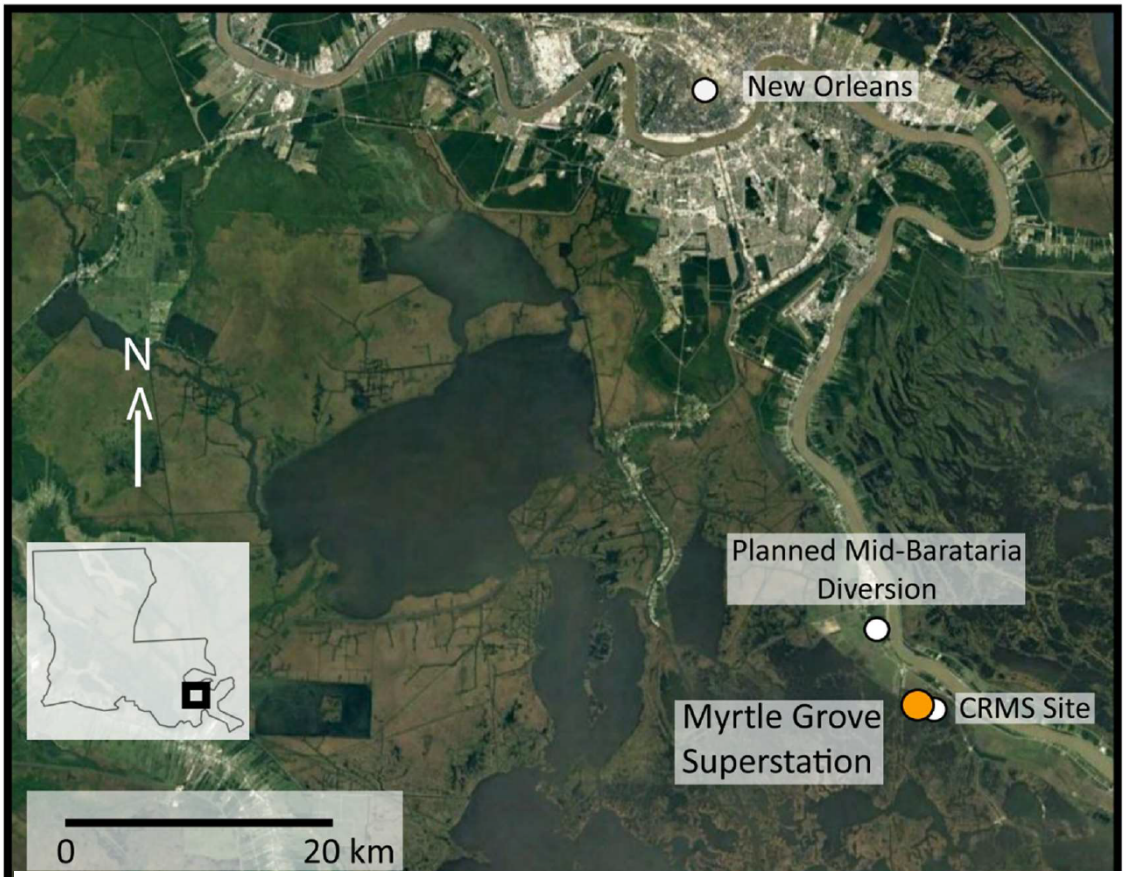

Figure 5. *Myrtle Grove Superstation sample site. 5 km south of planned Mid-Barataria sediment diversion. CRMS monitoring system for surface elevation change, vertical accretion and shallow subsidence rates. (Bridgeman 2018)*

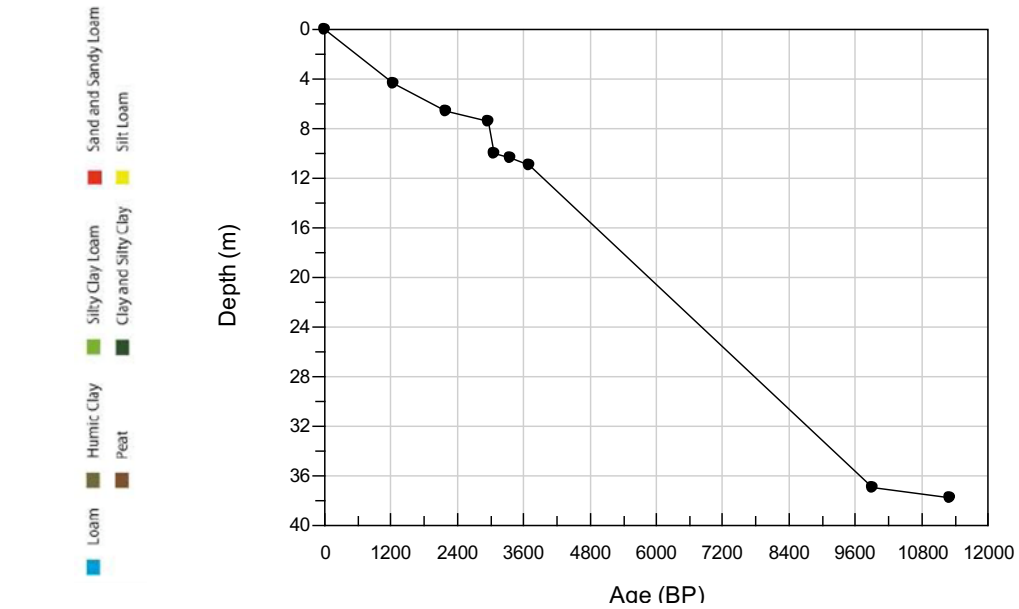

Figure 6. *Age depth plot from created from Bridgeman (2018) dated organic material. Zones added. Age model is based on radiocarbon and OSL dating. Sedimentation rate us assumed to be constant between points.*

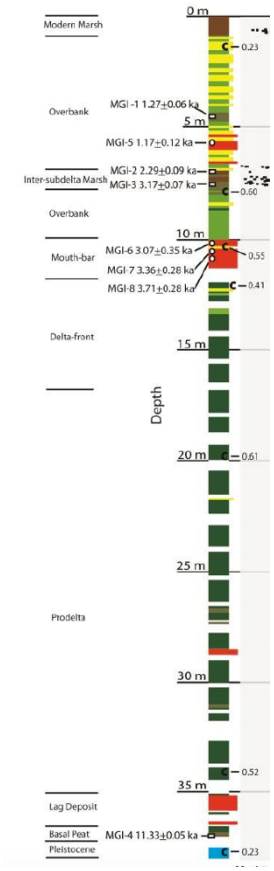

Figure 7. *Lithology, dated depths and inferred depositional environment. From Bridgeman (2018).*

Initial lithology of the core (Fig. 7) has been described and interpreted by Bridgeman (2018). The 38.7 m core is largely composed of mud with a few significant sand and peat beds. The base contains a loam and basal peat that denotes the Pleistocene- Holocene transition. From 35 m to 12 m is a mud-dominated homogenous unit with silty clay laminations mm thick between 12 and 18 m. A distinct sandy loam occurs at 28 m that is interbedded with shell hash. The upper 12 m is bounded on top by the modern marsh surface, seen as a 0.8 m thick peat bed and a 1.8 m thick sand body at the base. Between the intervals of silt loam and sandy layers, a significant organic-rich bed of intercalated peat at 6.7 – 7.7 m is seen.

As the MRD depositional environments changed through the Holocene, as a response to climate, sea level and internal processes, the potential for carbon storage will differ. I therefore aim to test the following hypothesis:

> Floodplain and wetland deltaic environments provided the optimum carbon sequestration and storage in the Mississippi River Delta during the Holocene.

Through the use of lipid biomarkers, palynology and bulk sediment properties, I will develop a detailed understanding of environment change through the Holocene and expand on the study of Bridgeman (2018). To test this hypothesis and to achieve larger goals of this thesis, I aim to:

1. Reconstruct the environmental conditions of the inland Mississippi Delta, including marine transgression and sea level fluctuation during the Holocene.

2. Explore the Holocene carbon sequestration potential of the Mississippi Delta.

3. Methods

3.1 Bulk sediment properties

The C/N ratio and $\delta^{13}C$ of organic matter in sediments can give a first indication of the main source of organic carbon (OC). For example, the C/N ratio of higher plants is enriched in carbon relative to that of the marine produced organic matter and can therefore infer a terrestrial or marine environment (Waterson and Canuel, 2008). Modern-day land-derived OM has a C/N ratio of 14-20, whereas phytoplankton and aquatic macrophytes show a C/N ratio between 4-10 (Meyers and Teranes, 2001). Similarly, the $\delta^{13}C$ of organic carbon is lower for terrestrial organic matter (~ −28‰ to −25‰) than for marine plankton and seagrasses, −22‰ to −19‰ and 14‰ to −10‰, respectively (Hedges et al., 1997; Canuel and Martens, 1993). Samples were freeze-dried and homogenised using a mortar and pestle prior to analysis of TOC, total nitrogen (TN) and $\delta^{13}C$. On average, 0.3 g of the homogenized sample sediment was treated with 1 ml HCL for 24 hours to remove inorganic carbon. An Element Analyser (Fisons Instruments NA 1500) coupled to an isotope ratio mass spectrometer (IRMS, FinniganMat Delta Plus) was used to analyse TOC, TN and $\delta^{13}C$. TOC and TN is expressed as a weight percentage (wt.%) of the dried sediment. Molar C/N ratios are calculated using TOC and TN. $\delta^{13}C$ values are expressed relative to the Vienna Pee Dee Belemnite (VPDB) standard.

3.2 Biomarkers

The biomarker proxies I will use are derived from GDGTs, long-chain diols and n-alkanes. Biomarkers will be analysed to further investigate environment changes. For example, the ratio of branched and isoprenoid glycerol dialkyl glycerol tetraether (GDGT) lipids is used to determine the relative input of terrestrial material in marine sediments (Hopmans et al., 2004). This ratio is quantified in the BIT index and based on the assumption that branched GDGTs mainly occur in terrestrial environments while crenarchaeol, often the dominant isoprenoid GDGT, is produced in the marine realm. Furthermore, branched GDGTs record the environmental conditions under which they are produced in their molecular structure, where the number of methylations is related to air temperature, and the number of internal cyclisation and the position of the methylations are related to soil pH (Weijers et al., 2007; De Jonge et al., 2014). Similarly, long-chain diols can indicate freshwater water input (C_{32} diols) and marine environment production (C_{28} and C_{30} diols). The abundance of C_{32} 1,15-diol is consistently higher close to the coast, in particular river mouths, suggesting a fresh water source and subsequent river transport (Lattaud et al., 2017). In addition, the abundance of mid-chain C_{23} and C_{25} n-alkanes of non-emergent aquatic plants, in contrast to vascular plants

with longer C chains, lead to the creation of the P_{aq} proxy ratio to establish an aquatic vs higher plant source of organic carbon in an environmental sample (Ficken et al., 2000). The average chain length of long-chain n-alkanes can further differentiate in plant functional type, assuming that trees that grow under wetter conditions tend to synthesize shorter alkanes (C_{29}) than grasses in more arid regions (C_{31}, C_{33}).

Using results from the Element Analyser, appropriate weights could be chosen for biomarker analysis. Due to the high TOC of the surface sample 1 (0 m) 1.5 g of freeze-dried sediment was used, whereas in other samples the weights ranged between 4 and 9 g. Samples were subsequently extracted using accelerated solvent extraction (Microwave MEX system) with a 25 mL 9:1 (v/v) mixture of dichloromethane and methanol then dried over N_2. Samples were then filtered over a sodium sulphate column and acid hydrolysis methylated for fatty acid extraction. Within the neutral extract acid hydrolysis and derivatization was used to release fatty acids for analysis on the GC (HP 6890) with a constant pressure of 100 kPa. 2 mL 1.5N HCL/MeOH was added to the samples and refluxed for two hours at 70°C. 2N KOH/MeOH (1:1, v/v) and 2 mL DCM and 2 mL H_20 added then washed with 2 mL DCM and dried over N_2. Derivatization by dissolving the sample in DCM:MeOH 1:1 0 µl of 2 M trimethylsilyldiazomethane was added per 5 mg of sample and left to react for 30 minutes and dried over N_2. The sample was then cleaned over a silica 60 (pipette; Merck 60, 0.063-0.2 mm, 70-230 mesh; not activated) with an additional amount of Na_2CO_3 on top of the silica to neutralize potential excess acetic acid; elute with EtOAc 3 times the column volume and dried over N_2.

The extract was subsequently separated on an activated aluminium oxide column using the following solvents: Hexane:DCM (9:1, v/v), Hexane:DCM (1:1 v/v) and DCM: MeOH (1:1, v/v) apolar, neutral and polar respectively (Hopmans et al., 2016). The surface sample of 0 m (MG1) was split into two for biomarker analysis due to the high organic matter content. The apolar fraction was dissolved in the solvent Ethyl acetate. 20 µl for MG1 and 30 µl for the remaining samples and co-injected with 1 µl of an external squalene (63.8 µg/l) standard on-column on a gas chromatograph coupled to a flame ionisation detector (GC-FID, Hewlett Packard 6890 series). The GC-FID uses an oven program starting at 70°C and rising first to 130°C at 20°C min^{-1} and then to 320°C at 4°C min^{-1} and held for 20 minutes. Using Agilent Chemstation software, concentrations of n-alkanes were determined by relating their peak areas identified using retention times, with that of the squalene standard and then normalised against TOC.

An internal GDGT standard, synthetic C46, was added to the polar fraction extract and subsequently dissolved in 1.5ml hexane:isopropanol (99:1, v/v) and filtered with a 45 u µm polytetrafluorethylene (PTFE) filter. Analysis of the polar fraction was conducted via a high-performance liquid chromatography-mass spectrometry (HPLC-MS: 6130B MS, 1290 infinity autosampler and 1260 infinity pump) using a method enabling the separation of 5- and 6-methyl brGDGTs following Hopmans et al., (2016). Detection of peaks was selected via ion monitoring (SIM; Schouten et al., 2007) using m/z 744 for the internal standard, m/z 1302,

1300, 1298, 1296, and 1292 for isoprenoid GDGTs including crenarchaeol and m/z 1050, 1048, 1046, 1036, 1034, 1032, 1022, 1020 and 1018 for brGDGTs. Agilent Chemstation software was used to integrate peak areas and concentrations were normalised against TOC.

Diols within the polar fraction were derivatised by silylating an aliquot of the polar fraction using 10 µl pyridine and 10 µl N20-bis(trimethylsilyl)trifluoroacetamide (BSTFA) and heating to 60°C for 20 minutes and dried over N_2 stream. Samples were dissolved in Ethyl acetate. MG1 (100 µl), MG2 (30 µl), MG21 (10 µl) and the remaining 50 µl Samples were co-injected with varying amounts of squalene on column on the GC-FID. Samples were analysed using the same program as the apolar fraction.

3.2.1 Long Chain Diols

Long chain alkyl diols (LCD) are molecules composed of at least 28 C atoms and contain an alcohol group at C_1 and mid-chain positions (C_{12}, C_{13}, C_{14} and C_{15}) and occur universally in marine sediments (Lattaud et al., 2017). In the marine realm the dominant diols found are the C_{28} and C_{30} 1,13-diols, C_{28} and C_{30} 1,14-diols and C_{30} and C_{32} 1-15 diols (Rampen et al., 2014a) with C_{28} and C_{30} 1,14-diols known to be synthesised by the *Proboscia* diatom (Rampen et al., 2007) and *Apedinella radians* marine algae (Rampen et al., 2011). The C_{28}, C_{30} 1,13-diols and C_{30}, C_{32} 1,15-diols are thought to be synthesized by eustigmatophyte algae (Volkman et al., 1999) that however are rarely found in the marine environment. Various LCD indices have been developed upon the distribution and fractional abundance of each diol, for example the Sea Surface Temperature (SST) proxy (Rampen et al., 2012) and other proxies for palaeo-upwelling (Rampen et al., 2008) and salinity (Versteegh et al., 1997). The C_{32} 1,15-diol has been attributed to a potential continental source, with data showing a higher abundance at river mouths and estuarine sediments supporting this theory (Rampen et al 2014a; De Bar et al., 2016). The results of Lattaud et al., (2017) further provide evidence for this continental source, constraining the C_{32} 1,15-diol to freshwater river production and suggesting its potential for a proxy for the input of riverine organic matter. The use of the C_{32} 1,15-diol as a proxy for freshwater input from rivers and lakes in marine sediments was later validated by Lattuad et al., (2021). The proxy is based upon the abundance of the C_{32} 1,15-diol normalised against the sum of all 1,13 and 1,15-diols. Due to the known marine origin and *Proboscia* origin of the 1,14-diols these are excluded (Lattaud et al., 2017).

$$\%C_{32}1,15 = \frac{AC_{32}1,15}{AC_{32}1,15 + AC_{30}1,15 + AC_{28}1,13 + AC_{30}1,13} \times 100$$

Equation 1. *The equation for the C32 1-15 proxy by Lattaud et al., (2017). A stands for the peaks, and therefore concentration, of the diols.*

3.2.2 *n*-alkanes

Leaf wax *n*-alkanes are one of the most abundant biomarkers synthesised by terrestrial, aquatic and emergent plants (Cunlin et al., 2020; Bray and Evans, 1961). Long chain *n*-alkanes are an essential component of leaf waxes and primarily serve to prevent internal water loss (Eglinton and Hamilton, 1967). Their high abundance, resistance to natural degradation and the information on vegetation and climate they contain has led *n*-alkanes to be an important biomarker for palaeoenvironmental reconstructions (Shi et al., 2021). They have an odd-over-even distribution (which is important to later explain the CPI, where lower CPI indicates relatively more even-chained alkanes indicating higher maturity and more degradation), and long chain waxes >C_{27} that are considered to be derived from higher plants, whereas shorter chains are linked to aquatic plants (C_{21}-C_{25}) or peats (C_{25}) and microbes (>C_{21}). The majority of studies on n-alkanes focus on temperature (Wang et al., 2018) and precipitation (Hoffmann et al., 2013), due to the dominant controlling factor of vegetation growth and climate events for palaeoclimatology. Plants synthesise longer alkanase chains under conditions of low humidity and water availability, reflecting the purpose of the wax in preventing water loss (Hoffmann et al., 2013). This is captured in the Average Chain Length (ACL). The Hoffmann et al., (2013) study on Acacia and Eucalyptus trees along a humidity gradient showed that ACL correlated significantly with hydrological conditions, supporting the thought that water availability and evapotranspiration were the major drivers of leaf wax *n*-alkane chain length. Straight-chain compounds vary from C_{20} to C_{37} *n*-alkanes with a strong odd/even prevalence (Poynter et al., 1989). The ACL proxy can therefore be used, with lower values indicating a dominance of herbs and shrubs and higher ACL values indicating the presence of trees.

$$ACL = (C_{25}*25 + C_{27}*27 + C_{29}*29 + C_{31}*31)/(C_{25}+C_{27}+C_{29}+C_{31})$$

Equation 2. *Taken from Poynter et al., (1989) indicates how ACL values have been calculated*

The *n*-alkane proxy (P_{aq}) was proposed by Ficken et al., (2000) to reflect the sedimentary input of submerged/floating aquatic relative to that of emergent and terrestrial species. It was found that *n*-alkanes display the most significant difference between the three plant types, with terrestrial and emergent maximising at C_{29} or C_{31} and floating plants maximising at C_{23} or C_{25} *n*-alkane. The P_{aq} proxy therefore expresses the relative proportion of mid-chain (C_{23}, C_{25}) to long chain (C_{29}, C_{31}):

$$P_{aq} = (C_{23} + C_{25})/(C_{23} + C_{25} + C_{29} + C_{31})$$

Equation 3. *The equation for the Paq proxy by Ficken et al., (2000)*

For modern plants this proxy gives the following values: <0.1 for terrestrial plants, 0.1-0.4 for emergent plants and 0.4-1 for submerged/floating macrophytes (Ficken et al., 2000).

The carbon preference indice (CPI) is often use to characterise oil and evaluate the maturity of source rocks (Marzi et al., 1993) but it can also be applied and used to infer the fresh organic carbon stored in sediment. The formula from Marzi et al., (1993) revised from Bray and Evans (1961), uses the even-carbon number peaks as the denominator and the odd-carbon peaks as the numerator to give consistent and more meaningful results. Higher CPI values of >5 have been found to exclusively be produced by higher plants, whereas CPI values of ~1 are derived from algae and bacteria, as well as petroleum (Cranwell, 1973). CPI can therefore be related to freshness, with a deceasing CPI indicating depletion of *n*-alkane freshness and higher CPI indicative of fresh material (Zhang et al., 2010)

$$CPI = (C23 + C25 + C27) + (C25 + C27 + C29)/2 * (C24 + C26 + C28)$$

Equation 4. *The equation for the C32 1-15 proxy by Lattaud et al., (2017). A stands for the peaks, and therefore concentration, of the diols.*

3.2.3 GDGTs

Glycerol dialkyl glycerol tetraethers (GDGTs) are organic compounds found in the membranes of bacteria and archaea and are at the base of several paleoenvironmental proxies (Sinninghe Damste, 2016). Crenarchaeol, an isoprenoid GDGT, is specific for ammonia-oxidizing archaea belonging to Thaumarchaeota (Schouten et al., 2013). Branched GDGTs (brGDGTs) are made by bacteria however the exact biological source remains unknown (Sinninghe Damste, 2011).

BIT

The findings that brGDGTs are produced and occur predominantly on the terrestrial environment, whereas crenarchaeol is the dominant GDGT in the marine environment led to the development of the branched isoprenoid tetraether (BIT) index (Hopmans et al., 2004). Based on the foundation that brGDGTs are produced in soils and transported by rivers to the coastal region, the fossilised brGDGTs found in coastal marine sediments can provide a record of past environmental changes of the coastal system and allow climate and environment reconstructions (Hopmans et al., 2004). The BIT index serves as a proxy for the relative abundance of terrestrial OM, with values closer to 1 representing soil and peat and values close to 0 for coastal marine and lake sediments (Schouten et al., 2013; Hopmans et al., 2004). The BIT index therefore can be used as a proxy for the relative abundance of fluvially-transported OM vs marine OM (Schouten et al., 2013).

$$\text{BIT index} = \frac{([\text{GDGT-I}] + [\text{GDGT-II}] + [\text{GDGT-III}])}{([\text{Crenarchaeol}] + [\text{GDGT-I}] + [\text{GDGT-II}] + [\text{GDGT-III}])}$$

Equation 5. *The equation to calculate the values of thr BIT Index.*

Rings tetra and IR

The foundation of many brGDGT proxies is the assumption that they are transported from the continent to coastal marine setting by rivers. However, this has been recently challenged by the findings of aquatic production of brGDGTs in rivers (De Jonge et al., 2014b) and coastal settings (Peterse et al., 2009; Sinninghe Damste, 2016).

Developments of liquid chromatography methods have led to the discovery of penta- and hexamethylated brGDGTs, where the peripheral methyl group varies from 5 to 6 positions along the alkyl chain (De Jonge et al., 2014a; Dearing Crampton Flood et al., 2018). This development aided in the recognition of riverine brGDGT production, with the study of De Jonge et al., (2015) showing that substantial amounts of particularly 6-methyl brGDGTs in the Yenisei River are aquatically produced. Typically, 5-methyl brGDGTs are correlated to temperature whereas the 6-methyl isomers are correlated to soil pH (De Jonge et al., 2014a). The Isomer Ratio (IR) is therefore the relative amount of 6- vs. 5-methyl brGDGTs calculated according to De Jonge et al., (2014a). In soils, 6-methylated brGDGTs are used to identify PH, whereas in rivers they can indicate freshwater production. In-river production can be recognised when the IR is higher in river samples than in the catchment soils. Therefore, a higher IR can be used to indicate more a higher riverine production of brGDGTs (Sinninghe Damste, 2016).

$$\mathrm{IR} = (\mathrm{IIa}' + \mathrm{IIb}' + \mathrm{IIc}' + \mathrm{IIIa}' + \mathrm{IIIb}' + \mathrm{IIIc}')/(\mathrm{IIa} + \mathrm{IIb} + \mathrm{IIc} + \mathrm{IIIa} + \mathrm{IIIb} + \mathrm{IIIc} + \mathrm{IIa}' + \mathrm{IIb}' + \mathrm{IIc}' + \mathrm{IIIa}' + \mathrm{IIIb}' + \mathrm{IIIc}')$$

Equation 6. *The equation for IR proxy values according to De Jonge et al., (2014a)*

Furthermore, Peterse et al., (2009) observed that the number of cyclopentane rings increases towards the ocean indicating an in situ coastal production of brGDGTs. #rings$_{tetra}$ proxy shows an increase from river mouth to shelf break reflecting this increased production of brGDGTs away from the continent (Sinninghe Damste, 2016). Sinninghe Damste, (2016) found the #rings$_{tetra}$ varies from 0–0.7 in soils and >0.7 in coastal marine sediments. Where values exceed 0.4 it is likely the brGDGTs have marine and soil derived origin and influence. The #rings$_{tetra}$ has been calculated following Sinninghe Damste (2016):

$$\#\mathrm{Rings}_{\mathrm{tetra}} = \frac{[\mathrm{Ib}] + 2 * [\mathrm{Ic}]}{[\mathrm{Ia}] + [\mathrm{Ib}] + [\mathrm{Ic}]}$$

Equation 7. *The equation for* #rings$_{tetra}$ *proxy values according to Sinninghe Damste (2016)*

3.2.4 Alkenones

Alkenones are biosynthesised by Haptophyceae algae, notably the coccolithophorid *Emiliania huxleyi,* the most widespread species of coccolithophores in the oceans and thus the most likely dominant producer of alkenones (Brassell et al., 1986). *Emiliania huxleyi* exhibits a large temperature range (1-30°C) and is therefore present in most eutrophic zone environments (McIntyre, 1967). They have been reported in salinities as low as 11-12 ppt in coastal areas and as high as 38-41 ppt (Gebühu et al., 2021). In the Myrtle Grove samples, no alkenones were detected.

3.3 Palynology

Palynology is a useful tool in palaeoenvironment reconstruction allowing for the interpretation of past vegetation trends (pollen and spores), changes in marine productivity (dinoflagellate cysts and other aquatic remains) and climate. Moreover, palynomorphs analysed in a core taken from land can indicate when a marine transgression occurred. The presence of palynomorphs from marine or brackish organisms will be strong evidence for intervals during which land was submerged and can indicate sea level fluctuations (de Vernal, 2009). The presence of terrestrial palynomorphs only (and/or freshwater palynomorphs) will infer a terrestrial environment with no prolonged stages of flooding or marine inundation. Pollen grains represent both local and regional source areas, allowing for the interpretation of the M.G. sample site but also that of the headwater signal and upland catchment area. The morphology of pollen grains and the knowledge of modern plant species allow for the source site to be inferred. The morphology of *Pinus*, for example, features two air sacs for efficient wind dispersal and is therefore representative of a large regional area (Fig. 19). Pollen such as *Chenopodiaceae* record a more regional signal, as their morphology does not allow for long distance dispersal via wind. Pollen cycles (palynocycles) of coastal plant assemblages have been associated with sea level change (Poumot, 1989) and can trace phases of transgression and regression (Gonzalez and Lunpont, 2009). Marsh plants such as *Chenopodiaceae* are a common representative of halophytic plants in subtropical wetlands (Adam, 1990). Salt marsh species first colonise bare zones of lower/middle marsh areas where there is a high incidence of inundation and disturbance from waves is frequent (Ranwell, 1972). As sea level rise decelerates, these pioneer species are able to permanently establish and act as sediment and organic matter traps that aid in further stabilising sediments and increasing the tidal height (Gonzalez and Lupont, 2009). *Ambrosia* is another known species characterising the build-up of a marsh environment (McDonald and Barbour, 1974). It must however be noted *Ambrosia* is a prolific pollen producer and can be transported great distances by the wind and therefore may not represent the local environment but a more regional area (McAndrews, 1988). The backswamp or marsh of deltas are continuously flooded environments that support wooded

vegetation, with clay-sized sediments introduced by overbank flooding from distributary channels and local runoff (Fisk, 1952; Roberts and Coleman, 1989). Backswamp vegetation develops quickly and supports wetland trees, including *Quercus*, and aquatic plants (Roberts and Coleman, 1989).

The modern-day assemblages of the Gulf of Mexico (Limoges et al., 2013) can aid in the identification and interpretation of dinoflagellate cysts. Common dinocysts in the GOM are Polysphaeridium *zoharyi*, Brigantedinium spp., Spiniferites *bentorii*, Operculodinium *centrocarpum* and Lingulodinium *machaerophorum.* Dinoflagellate cysts can be used to infer environmental conditions. P. *zoharyi* shows a clear trend of increased abundance at shallower depths and this affinity for nearshore depths may be related to many parameters. Nutrient affinity, salinity, turbulence, water stratification and light penetration, though difficult to quantify, may influence the relative abundance of P. *zoharyi* (Limoges et al., 2013). Brigantedinium spp. has been well correlated to increasing water depth. P.*zoharyi* and Brigantedinium spp. both dominate the assemblages of the modern day and are therefore expected to be present in the MG study area. In modern sediments, *L. machaerophorum* is often found in coastal estuarine environments and thrives in nutrient-rich conditions. Many nutrients arrive to the nearshore in the form of sediment transported from the terrestrial realm by rivers. The relative abundance of *L. machaerophorum* can therefore indicate a river-dominated marine environment (Zonneveld et al., 2013).

22 samples were processed in the Palynology Laboratory of University Utrecht. Using a mortar and pestle, roughly seven grams of the sample were crushed into ~2.5mm particles. One *Lycopodium* tablet containing 19855 spores was added to each sample with Agepon 1:200. 10% of hydrochloric acid (HCl) was gradually added to remove carbonates from the sample until a reaction was no longer noticeable. Water was added to fill the remaining tube and left to settle overnight before being centrifuged at 2200 RPM for 5 minutes, acc 9, dec 6 then decantation and refilling of water. For some samples the deceleration was left at 0 to ensure complete separation of sediment and liquid. Samples were then transferred to the HF lab. Hydrofluoric Acid (HF) is used to remove silicates such as sand and clay from the samples. HF 40% was added gradually in four steps as the reaction can be volatile. Samples were then shaken for 120 minutes at speed 250RPM then left to settle overnight. Directly after HF it is important to rinse with HCl to break up clumps from the HF cycle. 30% HCl was added and if space, filled with water to a centimetre below the top. Samples were then centrifuged again at 2200 RMP for 5 minutes. Decantation as far as possible followed before adding water. This was repeated three times. Samples were then sieved in an ultrasonic bath using first a 100 µm sieve followed by a 10 µm sieve. Residues of 22 samples were mounted on glass slides using glycerine jelly and analysed using a light microscope at 40x magnification. Due to time constraints 12 slides were counted with an average of 250 pollen grains identified and recorded. Due to the relative lack of dinocysts in the assemblage they were counted up until the end of the slide. The reliability of the dinocysts counts must be taken into account as samples 36 and 35 have a total of <100 dinocysts counted however this greatly reduced to an

average of ~15 for the following samples. Dinocysts were identified using Zonneveld and Pospelova (2015), Rochon et al., (1999), Boyd, (2016) and Limoges et al., (2010). Pollen grains were identified using Willard et al., (2004). The program C2 (Juggins, 2007). will be used to create stratigraphic diagrams of pollen, dinocysts and perform a PCA analysis.

Pinus is the dominant pollen grain across samples, it was therefore excluded when calculating percentages of single species. A known amount of lycopodium was added to the slide enabling pollen concentrations to be calculated. To calculate pollen concentrations, a multiplication value, lycopodium counted/lycopodium added, was multiplied by the absolute pollen value and divided by slide weight. The groups Arboreal, Herbs, Wetland trees and Aquatic plants have been created to compare assemblages of similar pollen species. Arboreal is made up of *Pinus, Picea, Fagus, Quercus, Tsuga, Caprinus, Ulmus, Carya, Juniperus, Corylus, Nyssa*. Herbs: *Poaceae, Astraceae Tubiliflorae, Chenopodiaceae, Artemisia, Ambrosia, Plantago, Myrica cerifera.* Wetland*: taxodium, Alnus, Liquidambar, Nyssa, Cyperaceae Sagittaria, Sphagnum*. Aquatic plant: *Nuphar, Typha*. Total Spiniferites include the species S. *bentorii*, mutated low-salinity Spiniferites and Spiniferites that could not be identified to species level.

3.3.1 Statistical Analysis

Principal component analysis (PCA) was performed, using C2, on all pollen and dinocyst species to reveal the distribution of taxa in relation to ecosystem development. Taxa are categorised into statistically meaningful groups and provide a foundation to verify coastal environments. Percentage data from the palynomorph analysis, except *Pinus*, were used in the PCA. Total number of samples is 12 with 43 variables included in the model. PCA will be plotted against depth in C2.

4. Results

4.1 Bulk sediment properties TOC, C/N and δ^{13}Corg

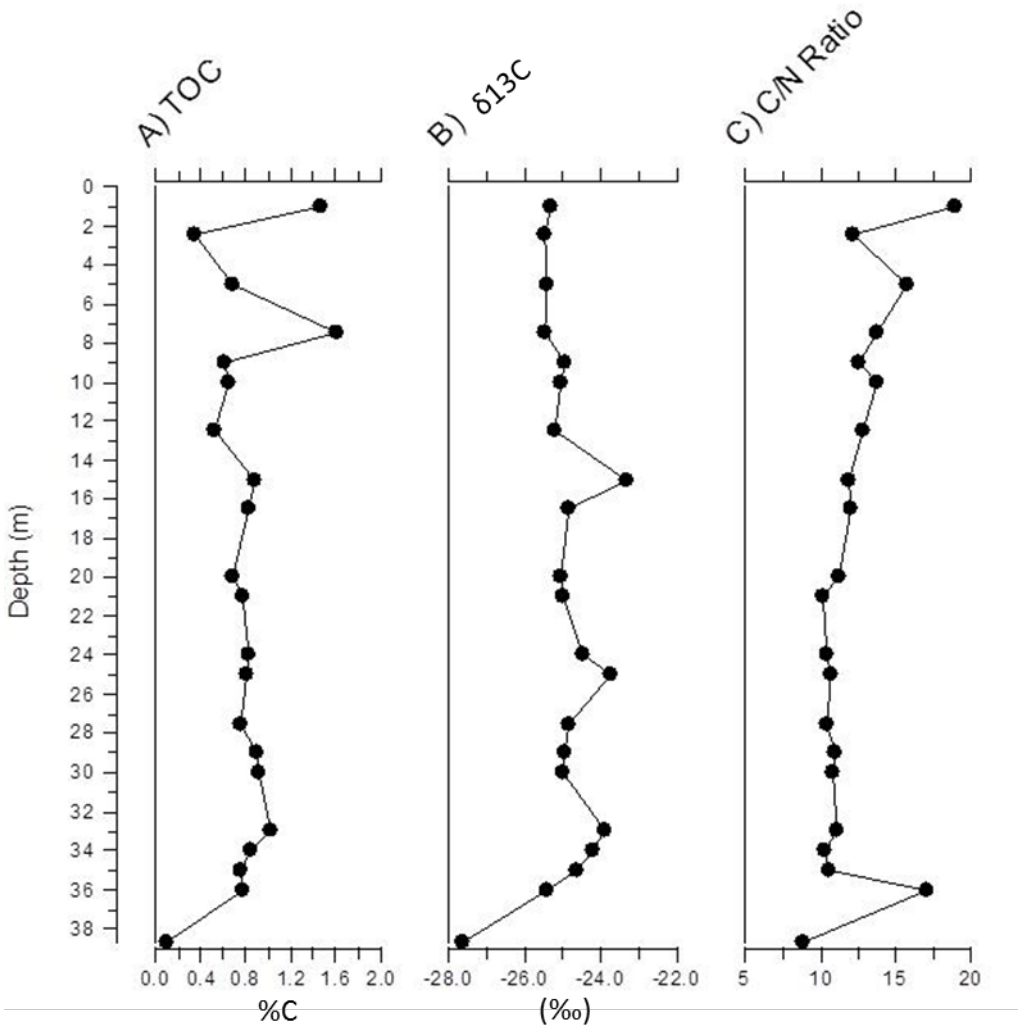

Figure 8. *Bulk sediment properties: A) Total organic carbon %C (TOC), B) δ^{13}C‰, C) C/N ratio. Values from 0m have been excluded.*

Total organic carbon (TOC) ranges between 0.1–1.61, with continuous values of ~0.8 between 36 and 9m that follow a sharp increase from 0.1 to 0.7 at 36 m. After 9 m values are no longer constant, peaking to 1.6 at 7.5 m and 1.47 at 1 m. δ^{13}C values vary between -27.6‰ and -23.3‰. An increase from -27.6‰ to -23.8‰ between 38.7 m and 33 m characterizes the bottom of the core. δ^{13}C values are mostly constant at -25‰ with marked peaks at 25 m and 15 m reaching ~-23.5‰. C/N ratios range between 8.9 and 18.9. A sharp peak at 37 m of 17.1, rising from 8.9 at 38.7 m is clear. From 35 m to 5 m a gradual increase is evident with values rising from 10 to 15.7. At 2.5 m values fall to 12.1 before again peaking to a high of 18.9 at 1 m. Values at 0 m have been excluded as they show an anomaly to the data trends of very high values.

4.2 Lipid biomarker concentrations and proxies

4.2.1 Long Chain Diols

Total diols have a range between 111 and 6 μg/g peaking at 34 m at 111 μg/g before decreasing to an average of 10 μg/g between 24 m and the surface. The C_{30} 1,13 diol concentration range is the lowest with values between 0 and 2 μg/g, the highest concentrations between 1 and 50 μg/g is found in C_{30} 1,15. The C_{28} 1,13-diol, 1,14-diol, C_{30} 1,14-diol and 1,15-diol all show a similar pattern with very low (>5 μg/g) or no presence after 24m and a well-defined peak at 35m. The C_{30} 1,13-diol shows the most variation. A peak at 35m is seen but unlike the previous diols it is not the maximum. Values gradually increase before reaching the highest value of 2.29 μg/g at 16.5 m. A stepped decrease follows reaching a low of 0.15 μg/g at 2.5 m before increasing to 2 at the surface. The C_{32} 1,15-diol peaks at 34 m reaching the highest value of 28.9 μg/g before decreasing and peaking again at 30 m reaching 20 μg/g. Values gradually decrease towards 24 m before remaining at a constant of ~7 μg/g with small peaks reaching ~8.5 μg/g at 7.5 m and 1 m respectively. The C_{32} 1,15-diol, a proxy for the input of riverine organic matter shows an overall increase, rising steadily from 13 μg/g at 38.7 m to 51.3 μg/g at 9 m. A sharp increase to 77.4 μg/g at 7.5 m is followed by a decline to 41 μg/g at 2.5 m.

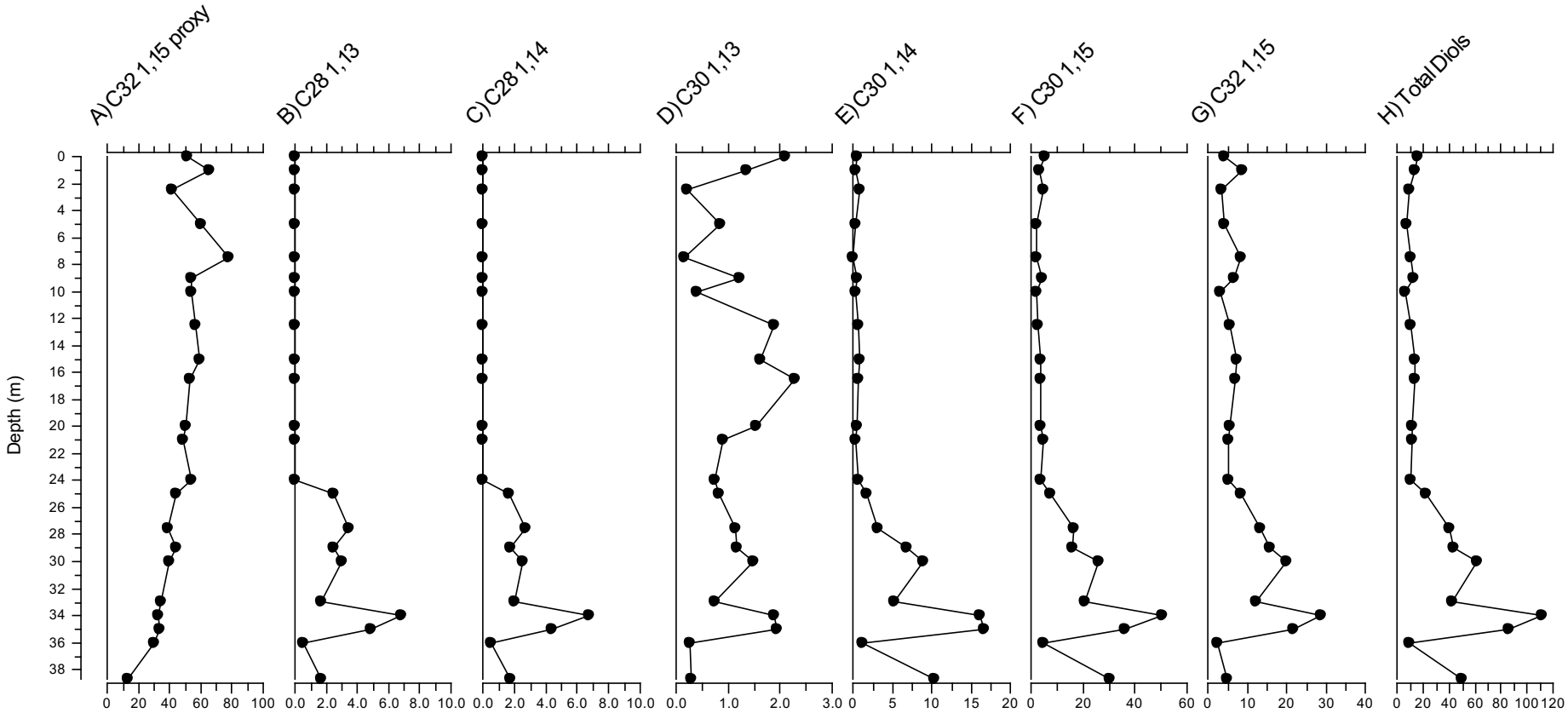

Figure 9. *Concentration of the six diols studied (µg/g OC). A) C32 1,15 proxy (also FC32 1,15), B) C28 1,13, C) C28 1,14, D) C30 1,13, E) C30 1,14, F) C30 1,15, G) C32 1,15, H) Total diols*

4.2.2 n-alkanes

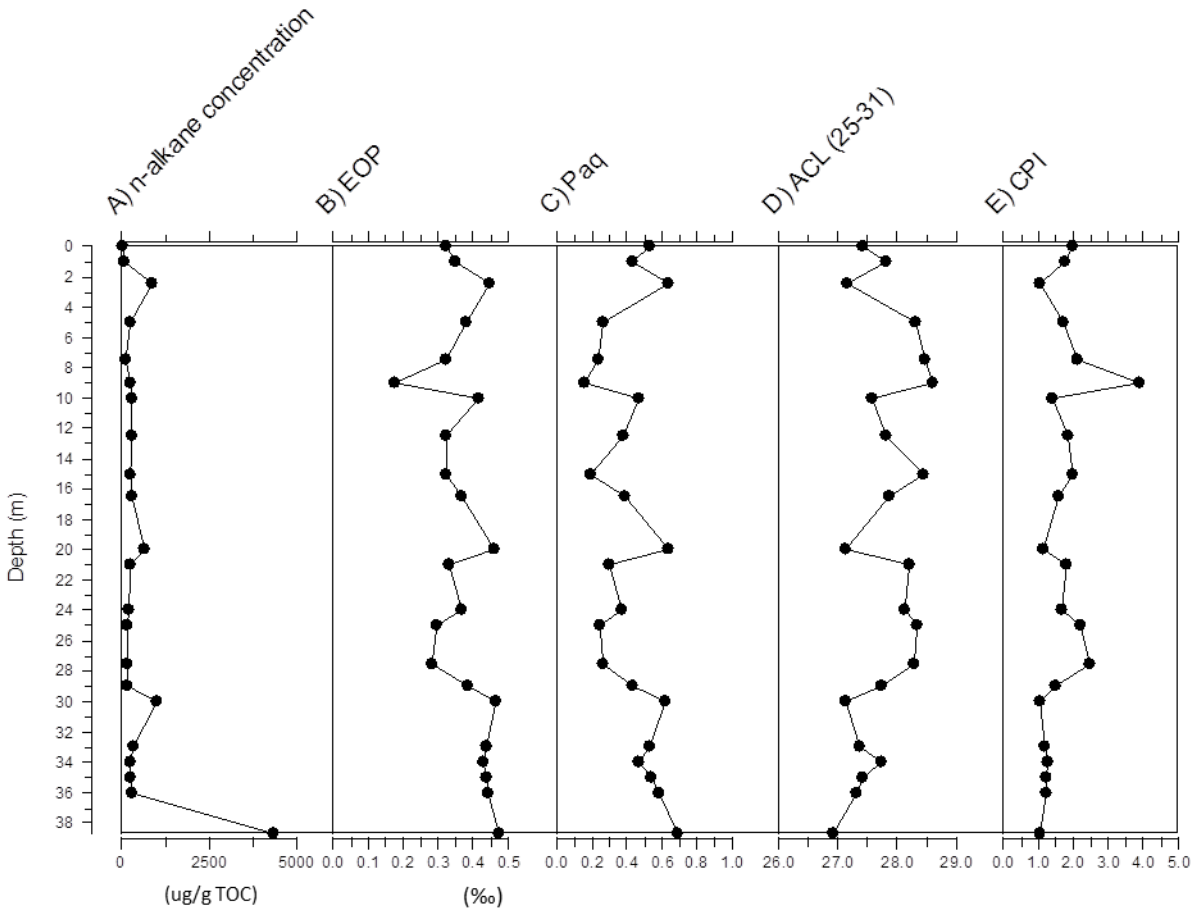

Figure 10. *A) n-alkane concentration (µg/g TOC , B) Even-over-odd (EOP) predominance (‰), C) P_{aq}, D) ACL (25-31), E) Carbon Preference Index (CPI)*

Chain lengths of n-alkanes present in the samples ranges between C_{21}–C_{33}, with C_{33} only present at 9 m. n-alkanes are present in all samples, but in varying concentrations. The clearest is at 38.7 m with a concentration of 4336 µg/g that decreases significantly to 330 µg/g at 36 m. Concentrations above 1000 µg/g are not seen again after 38.7 m. A small peak to 1000 µg/g at 30 m and 900 µg/g at 2.5 m deviates from the average of 250 µg/g. The even/odd predominance (EOP) shows samples where odd chain lengths are dominant in the samples. When the even/odd chain length distributions of n-alkanes are similar, a value of 0.5 is shown. Lower values will signify an odd chain length dominance. This occurs between 25 and 20 m with values of ~0.3 and at 9 m with a significant dip to 1.77 before returning to 0.5 by 2.5m.

The P_{aq} proxy, accounting for the input of submerged/floating freshwater macrophytes, varies between 0.1 and 0.7. The highest value of 0.68 is at 38.7 m before a slow decrease to 0.24 at 25 m. Values then increase to 0.63 at 20 m before a stepped overall decline to the lowest value of 0.19 at 15 m and 0.16 at 9 m. A final peak of 0.63 at 2.5 m shows a sharp increase.

The ACL proxy, used to indicate the vegetation type, shows an almost opposite trend of the P_{aq} proxy. Average chain lengths vary between 27 and 29. At 30 m, values rise from 27.1 to 28.3 and remain constant for 10 m before falling back to 27.1 at 20 m. A second, shorter-lived peak at 15 m to 28.4 correlates to the decrease seen in the P_{aq} proxy. A third prolonged peak between 9 and 5 m at values of 28.4 precedes a decrease to 27.4 at 0 m. The CPI, a proxy for fresh OM, varies between 1 and 4. Values begin low and constant at 1 between 38.7 and 30 m before increasing to 2.48 at 27.5. Values return to 1.13 at 20 m. A sharp peak to a high of 3.87 at 9 m is followed by a gradual decrease back to 1 at 2.5 m before a small increase to 2 at 0 m.

Fatty acids were also measured but not used in this thesis, the results are therefore shown in the Appendix (App. 1).

4.2.3 GDGTs

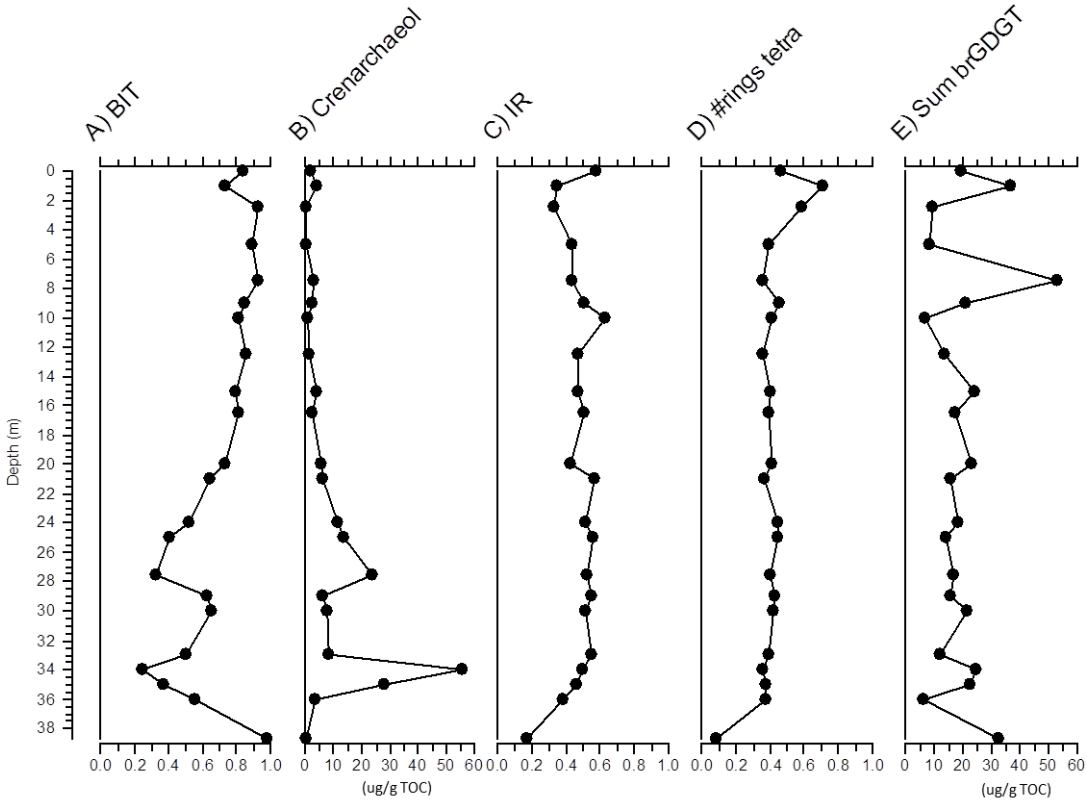

Figure 11. *A) BIT Index. B) Crenarchaeol concentrations (µg/g TOC), C) Isomer Ratio (IR), D) #ringstetra, E) sum of brGDGTs (µg/g TOC)*

GDGTs are present throughout the core. IsoGDGTs are largely dominated by crenarchaeol and increase with depth. Total brGDGT concentrations show a general decrease with depth. The sum of brGDGTs show a decrease from 32 µg/g to 6 µg/g at 38.7 to 36 m. Values then remain relatively constant at ~20 µg/g. At 10 m values increase from 7 – 53 µg/g at 7.5 m before falling

back to 8 μg/g at 5. A second peak follows at 1 m with values reaching 36 μg/g before again falling to 20 μg/g at 0 m. Crenarchaeol, the dominant GDGT in the marine realm, peaks at 34 m and 28 m to 55 and 24 μg/g respectively, before a gradual decrease from 24 to <5 μg/g towards the surface.

As a result, the BIT index, which indicates the relative abundance of fluvially-transported soil OC vs marine OC, varies between 0.24 and 0.98. The BIT index begins at 0.98 at the bottom of the core (38.7 m) and then decreases to the lowest overall value of 0.24 at 34 m. At 29 m a slow increase to 0.63 precedes another sharp decline at 27.5 m to 0.32. From 27.5 m there is a gradual increase of the BIT index from 0.32 to a high of 0.93 at 2.5 m before a further decrease to 0.73 at 2 m. The isomer ratio (IR), an indicator for fluvial brGDGT production, varies between 0.17 and 0.57. A gradual increase from 0.17 at 38 m to 0.5 at 34 m is followed by relatively constant values of ~0.5 until 5 m. A sharp increase from 0.35 to 0.6 between 2–0 m follows. The $\#rings_{tetra}$, a proxy to identify marine production, varies between 0.09 and 0.7. The IR increases from 0.09 to 0.4 between 38.7 and 36 m then constant values of 0.4 follow until 7.5 m. In the upper 5 m, the IR increases from 0.4 to 0.7, and then decreases to 0.46 from 1–0m.

4.3 Palynology

4.3.1 Dinoflagellate cysts

Dinocyst abundance and concentrations are far lower than pollen, with dinocyst concentrations ranging between 28 and 874 dino/g. The concentration per gram of pollen is almost five times the amount of dinocysts per gram, showing the dominance of pollen grains in the palynology assemblage. Dinocyst concentrations peak at the bottom of the core at 36 m before sharply declining to 63 dino/g at 30 m. Peaks to 230 and 269 dino/g at 27.5 and 16.5 m respectively deviate from an average of >100 dino/g between 30 and 7.5 m. A final peak to 372 dino/g at 1 m is seen at the surface. Dinocysts per gram show a decreasing trend from 6 to 30 m with a small increase at 27.5 m reflecting the trends of P. *zoharyi*. The small peak at 16.5 and 1 m is contributed by *Acritarchs* and *Echinidinium*. *Polyspaeridium zoharyi*, Total *Spiniferites* and *Operulodinium* show similar patterns. The most abundant species is P*. zoharyi* with a maximum of 32% at 36 m that sharply decreases to >1% by 30m before a small increase to 6.7% at 27.5 m. From 25 m P*. zoharyi* is no longer seen in the record. Total *Spiniferites* highest value of 16% also occurs at 38.7 m before a sharp decline to >1% at 30 m before an increase to 5% by 27.5 m. *Operulodonium* is not present (0.5%) at 36 m but reaches its maximum of 9% at 35 m before a similar decline to >1% by 30 m and subsequent increase to 2.5% by 27.5 m. *Lingulodinium machaerophorum* shows highest values of 4.6% at 35 m before decreasing to values not exceeding 2% and disappearing past 16.5 m. Acritarch concentrations show an opposing trend by not being present in the lower core and appearing at 16.5 m at 3%, increasing to the highest value of 11% at 1 m.

4.3.2 Pollen

Pollen per gram values vary between 1628 and 4610 with the lowest values seen at 36 m. Values peak to above 4000 at 35 m and 16.5 m. Values stay relatively high ~3000 in the lower core between 35 m and 24 m before decreasing to ~2000 in at 10 m. An opposing trend in the assemblage is seen at 36 m where dinocysts peak and pollen grains are the lowest. The most dominant group is herbs at least 35% of the total pollen assemblage at all times. Herbs begin low at 36 m with 37% before steadily increasing towards a peak of 75% at 33 m. A subsequent decrease to 50% at 25 m precedes another increase to a high of 79 % by 20 m. A decrease to 47% at 16.5 m is then followed by a gradual increase to 74% between 10 m and 1 m. Arboreal vegetation fluctuates between 13–47%, beginning high with 34% at 36 m before a steady fall to 14% by 33 m. Values peak at 16.5 m to 47% before a gradual decline to 13% at 1 m. Wetland tree values remain under 20 % with the highest value of 16.6% at 36 m. A stepped decrease to 1% at 27.5 m is followed by a sharp increase to a peak of 13.5% at 25 m before returning to >2% until 10 m. A gradual increase follows to 14% at 7.5 m ending with a small decline at 1 m to 11%. Aquatic plants make up the smallest contribution to the assemblage. Again, the highest value is of 36 m is at 11% before a staggered fall to 0.9% by 25 m. A small increase to 6% into 24 m is followed by a decrease seen to >3% until 0 m.

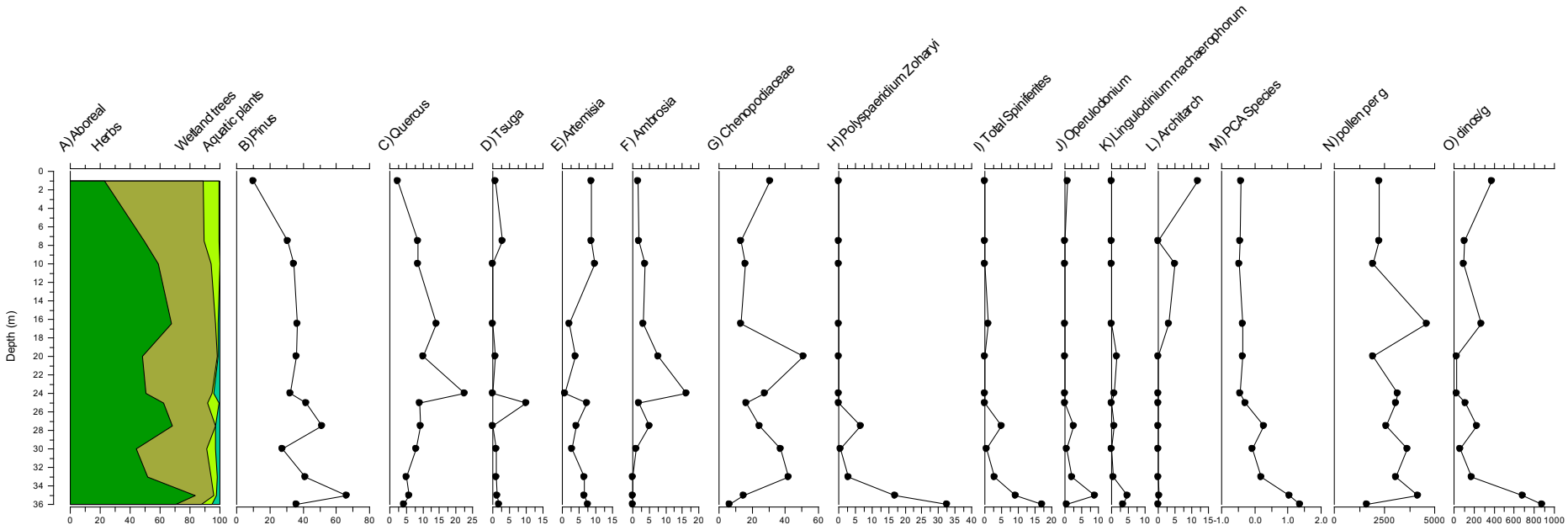

Figure 12. *Pollen diagram of A) Grouped Taxa (Arboreal, Herbs, Wetland trees and Aquatic plants), B) Pinus % of assemblage. C-O are % of assemblage excluding Pinus.*

Chenopodiaceae is the dominant pollen grain in the assemblage. At 36 m *Chenopodiaceae* starts at >10% and increases to 41% by 33 m. A gentle decrease to 16% at 25 m is followed by another increase and a maximum peak of 50% by 20 m. A fall to 13% at 16.5 m is followed by constant values of ~15% until a small increase to 30% at 1 m. *Quercus* percentages gradually increase from 4% to 9% between 36 m and 25 m before a sharp peak at 24 m to 22%. Values return to >10% at 20 m before a second peak of 14% at 16.5 m that precedes a slow decrease between 2% at 1 m. *Artemisia* values remain below 10%, decreasing from 7% at 36 m to 3% at 30 m. A peak to 7% at 25 m before falling to >1% at 24 m precedes a stepped increase with values reaching up to 9.5% 10 m then remaining up to 1 m. *Ambrosia* values generally remain below 5% and are not present until 30 m. A sharp peak to 16% at 24 m gently decreases back to >5% from 16.5 m to 1 m. A trend can be noticed, with a peak in *Artemisia* at 25 m, followed by a peak in *Ambrosia* at 24 m and finally a peak in *Chenopodiaceae* at 20 m. *Tsuga* values remain low (>3%). Until 25 m they do not exceed 2% where a peak reaching 10% correlates with the fall in *Chenopodiaceae* at the same depth. At 7.5 m *Tsuga* returns to >3% after an interval of no occurrence (16.5-10 m).

4.3.3 Statistical Analysis

On the PCA biplot the eigenvalue for axis 1 and axis 2 is 0.35209 and 0.19432, respectively. Along PC1 axis *Polyspaeridium zoharyi*, a marine dinocyst, has the highest positive loading, whereas terrestrial shrubs and tree species (*Poaceae*, *Quercus* and *Chenopodiaceae*) have the highest negative loadings. It is likely that PC1 represents a salinity gradient, with salinity increasing towards the positive end of the axis. On PC2 *Cyperaceae* has the highest positive loading whereas *Chenopodiaceae* shows the highest negative loading. The *Cyperaceae* value stands out as it does not fit the trend. The reliability of this value then must be called into question as, compared to the other species, the absolute count value is low. With PCA 2 featuring *Sphagnum* and *Pseudoschizea*, a peat moss and freshwater algae, at positive values and *Chenopodiaceae* and *Poaceae* with negative values, it is reasonable to infer that PC2 represents a hydrological regime gradient relating to moisture content. PC1 has been plotted against depth in Fig. 12. Values begin high of 1.36 at 36 m and decrease steadily to -0.08 by 30 m. A small peak to 0.26 at 27.5 m before another decrease to >1 is seen from 25 m to the surface. The trend of PC1 follows a similar pattern as that of the dinocyst concentration.

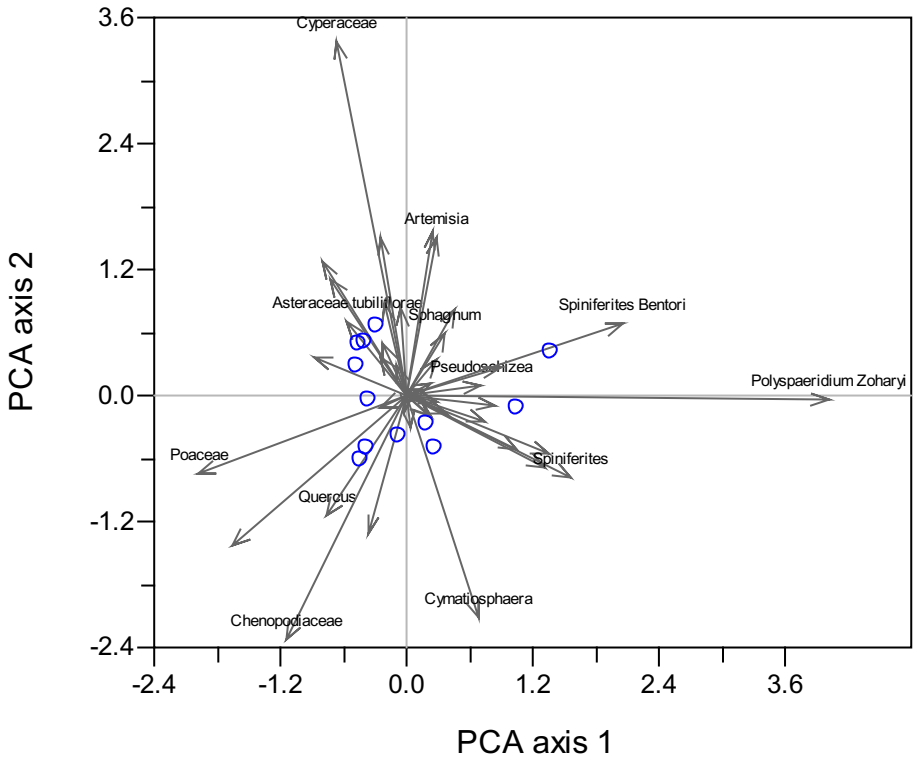

Figure 13 *PCA species biplot analysis, PCA axis 1 has been interpreted to plot positively for marine/salinity elements. PCA axis 2 plot has been interpreted to plot positively for moisture content. Plot was made using the program C2.*

5. Discussion

5.1 Stratigraphical zones

Using the lithological units, Bridgeman (2018) was able to broadly classify and interpret likely environments of the inland Mississippi River Delta. The basic interpretation from Bridgeman (2018) will be expanded upon through the use of biomarkers, palynology and bulk sediment analysis.

From the supporting lithology and trends seen in the data, five zones have been recognised. Zone 1, within Pleistocene basal peat and subsequent clay lithology, spans between 38.7 and 27 m and is recognised primarily through the overall sharp decrease in TOC, $\delta^{13}C$ and the BIT index. Three sub-zones 1c, 1b, and 1a are represented in grey where the BIT index, C_{28} and C_{30} 1,14-diols and dinocysts concentration diverge from the overall trend. Zone 1c, 37.8 to 33 m, is defined by a rapidly increasing $\delta^{13}C$ and decreasing BIT index. Zone 1b is characterised by a subsequent reversal of these previous trends and a significant drop in grain size, primarily a decrease in sands, at 35 m, and an increase in silt at 34 m showing a slight environment change (Bridgeman, 2018). Zone 1c is recognised by another fall in the BIT index and an increase in dinocysts. Zone 2 is between 27 and 19.5 m and within the clay lithology with no clear lithological changes. This zone is however recognised in the BIT index, gradually rising, and a peak in pollen such as *Tsuga*, *Artemisia*, *Ambrosia* and *Chenopodiaceae*. Zone 3 includes the first lithological change from clay to sand and is bound by the zone spanning between 19.5 and 9.5 m. Within the data set, this zone is recognised by an increase in C/N ratio and a steadily increasing BIT index and $F_{C32\ 1,15}$ with a varying P_{aq} and ACL proxy values. Zone 4, between 9.5 and 2 m, contains an ever-changing lithology of clay, sand, silt and peat. This zone is recognised by an increasing C/N ratio and P_{aq}, a peak in TOC, CPI, brGDGTs and $F_{C32\ 1,15}$. The $F_{C32\ 1,15}$ decreases after the peak at 7.5 m, the lowest value bound by the top of the Zone. IR shows a gradual decrease with $\#rings_{tetra}$ showing a significant increase. Zone 5, between 2 m and the surface, is recognised through sharp increases in both TOC and C/N ratio. The $F_{C32\ 1,15}$, brGDGTs and $\#rings_{tetra}$ all show a rise before a smaller fall, However the opposite is seen in the BIT index and IR. Within the lithology, a transition from sand to present-day peat is understood.

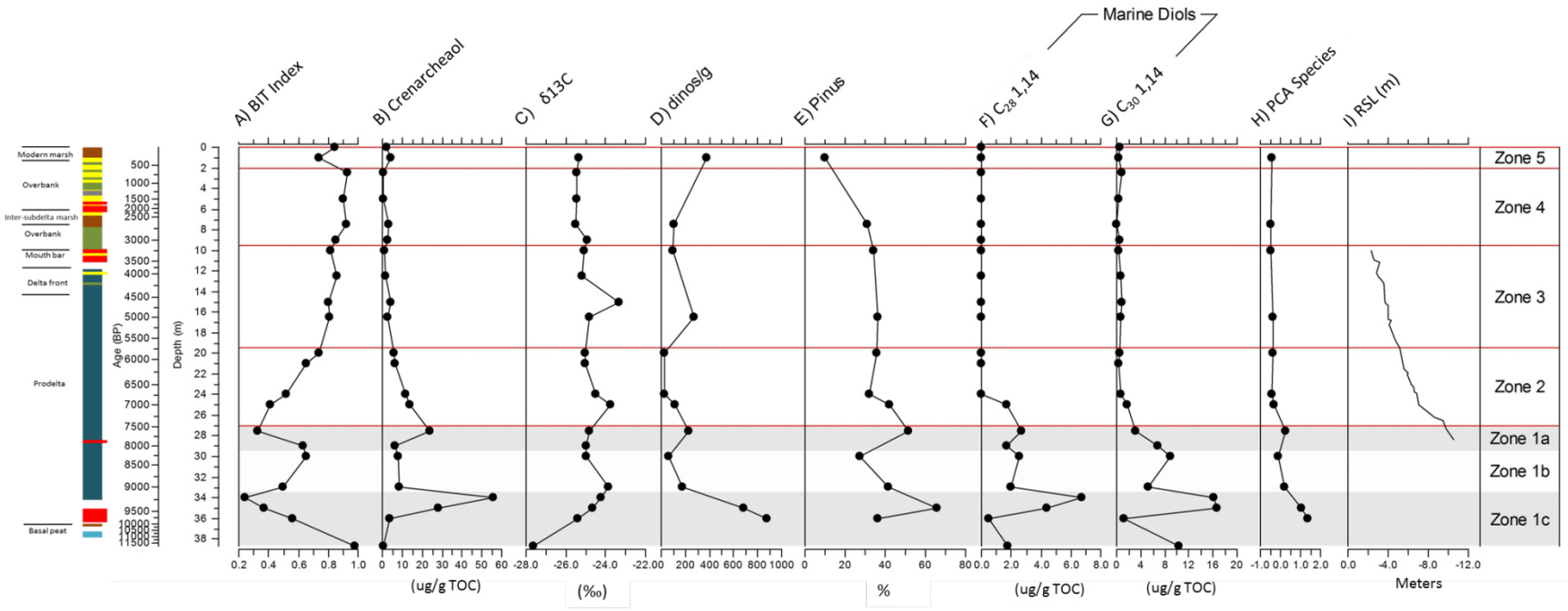

Figure 14. *Lipid biomarkers, palynology and bulk sediment property indicators with depth (m) and age (BP) highlighting the transgressive phase of the Holocene. Simplified lithology from Bridgeman, (2018). A) BIT Index, B) Crenarchaeol (µg/g), C) $\delta^{13}C$ ‰), D) dinos (per gram), E) Pinus, F) C_{28} 1,14, G) C_{30} 1,14, H) PCA Species, I) RSL (m)*

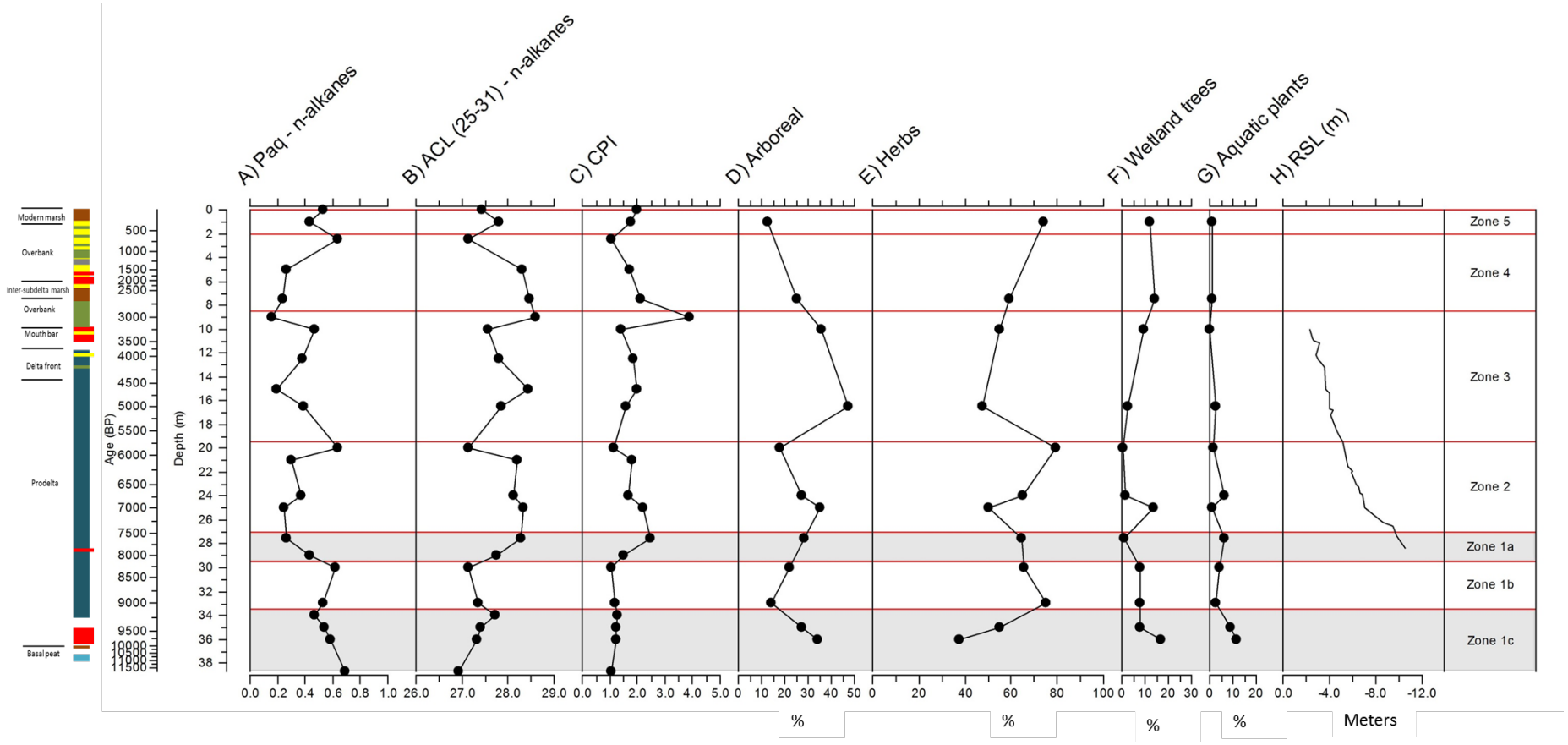

Figure 15. *n-alkane lipid biomarkers A) Paq, B) ACL and C) CPI with pollen groups (including Pinus), D) Arboreal, E) Herbs, F) Wetland trees, G) Aquatic plants, H) RSL*

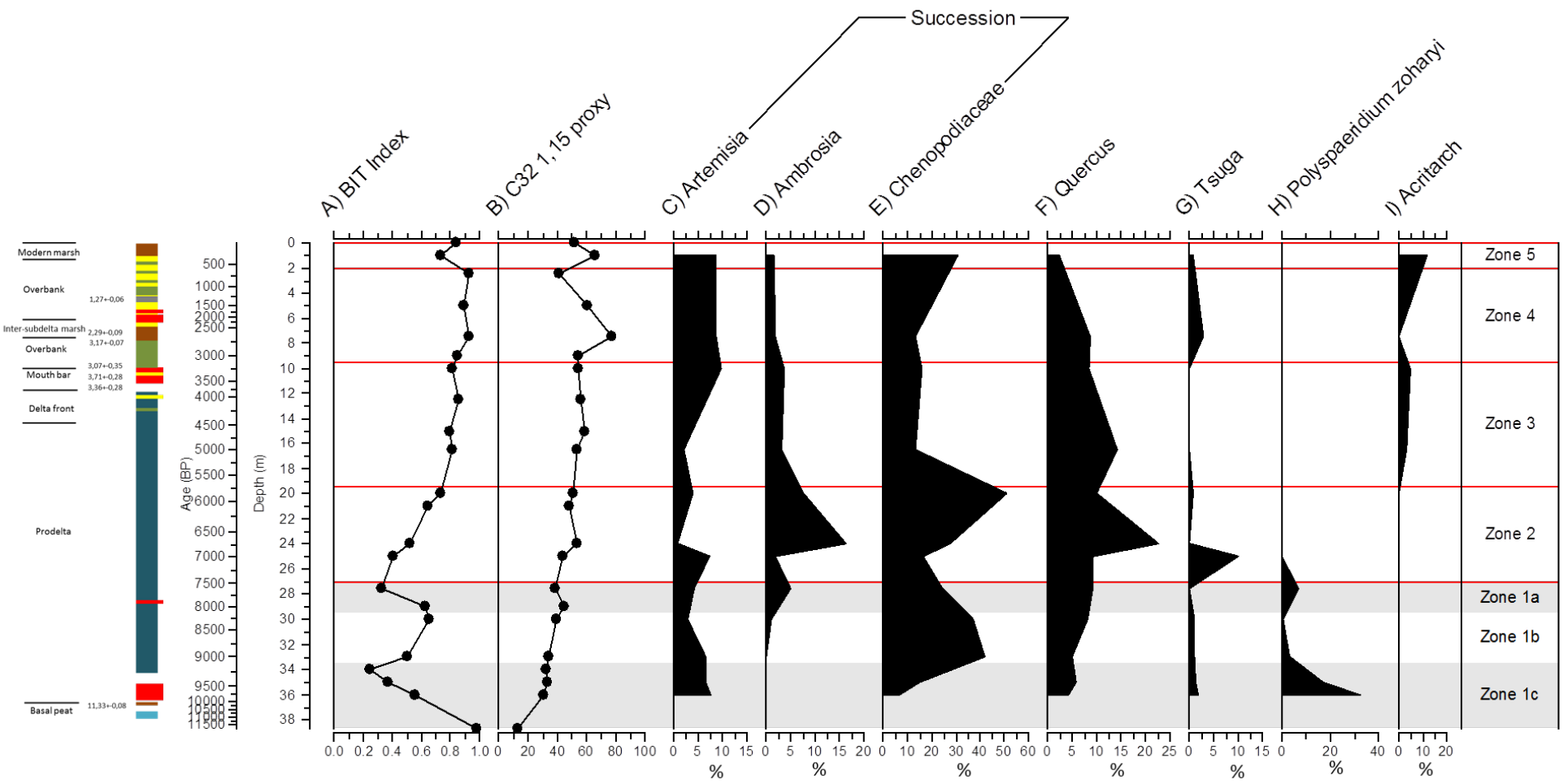

Figure 16. *Lipid biomarkers A) BIT Index and B) C32 1,15 proxy with most prominent palynology species. C) Artemisia, D) Ambrosia, E) Chenopodiaceae. F) Quercus, G) Tsuga, H) Polyspaeridium zoharyi, I) Acritarch*

5.2 Zone 1 – Zonal interpretation

5.2.1 Zone 1C - Zonal interpretation

Zone 1c is underlain by a basal peat that formed on top of the Pleistocene surface as sea level started to rise during the Early Holocene. At ~11.3 ka relative sea level was still below ~36.8 m, indicated by low salinity and macrofossils found in the basal peat. An intermediate environment was interpreted from the occurrence of both fresh and brackish marsh species (Louisiana Natural Heritage Program and Louisiana Department of Wildlife and Fisheries, 2009). Silty clay muds were deposited in a ~23 m thick deposit that has been interpreted as pro delta formations (Bridgeman 2018). Within the lower Holocene the primary depositional factor was sea level, however as sea level stabilised more complex internal delta processes were able to alter and influence the depositional history and present-day environments of the MRD.

The interpretation from Bridgeman (2018) of a pro delta deposit is supported by this study. A lithological unit of a primarily terrestrial Pleistocene clay at 37.8 m is supported by enriched $\delta^{13}C$ values of -28‰ that indicate a greater input of terrestrial OC (Hedges et al., 1997). A high (>0.9) BIT index at 37.8 m suggests a terrestrial environment, likely the result of a more distal coastline. Zone 1c highlights the initial transgression (Fig. 14), with the environment moving from terrestrial to marine. Through Zone 1c the increase of $\delta^{13}C$ values to -24‰ indicates a shift to a primarily marine origin of OC (Tyson, 1995). BIT index falling to 0.2 indicates a reduction of OM input at the study site inferring a marine environment. These trends within Zone 1c can be explained by SL rise leading to a marine transgression rendering the MG site submerged and further away from the coastline (Dearing Crampton-Flood et al., 2018), and therefore receiving significantly less terrestrial OM from fluvial transport. A sharp increase in crenarchaeol and C_{28} and C_{30} 1,14-diols within Zone 1c further supports a transgressive stage. These diols are known to be biosynthesised by the diatom genus *Proboscia* (Sinninghe Damste et al., 2013) and the marine algae *Apedinella radians* (Rampen et al., 2011). Crenarchaeol concentrations have been observed by Sinninghe Damste et al., (2013) to maximise on the shelf waters between 25 and 70 m. The concentration of *Pinus* in the pollen record can be used as a proxy for the distance to the coastline. Due to the morphology of *Pinus* grains (Fig. 19) it is readily subject to long distance transport (Delcourt and Delcourt, 1996), typically by wind. A domination of wind-dispersed pollen over fluvial-transported pollen in the assemblage suggests river transport of pollen, like organic matter, was lower at that time. A clear shift from a terrestrial input of organic matter to a more marine origin is clear.

The palynology in Zone 1c supports biomarker data and the interpretation of a transgressive phase. Dinocysts per gram is shown to be at its maximum within Zone 1c and decreases towards 34 m. Although a sharp decline in dinocysts may be seen as a regressive phase and fall in sea level, the assemblage of dinocysts is important to look at. The most dominant dinocyst in the assemblage is *P. zoharyi* and therefore exerts the most control over total

dinocyst trends. The dominant environmental factor over the distribution of dinocysts in the Gulf of Mexico is the water depth, or rather, the distance to the coast (Limoges et al., 2013). This allows for the distinction between oceanic and coastal environments. The study by Limoges et al., (2013) shows a clear trend of increasing relative abundance of *P. zoharyi* at shallower depths. Within Zone 1c it can be interpreted that sea level was rising to a maximum depth at 34 m, to a depth greater than *P. zoharyi* tolerance, and therefore a decline in abundance is observed. Modern records of the Gulf of Mexico can be used to aid interpretation. Edwards and Willard (2001) shows that *P. zoharyi* reflects an inverse relationship with water depth (Fig. 17). Other species that are commonly found in neritic to coastal warm temperature environments are *Operculodinium centrocarpum* and *Spiniferites* (Limoges et al., 2013).

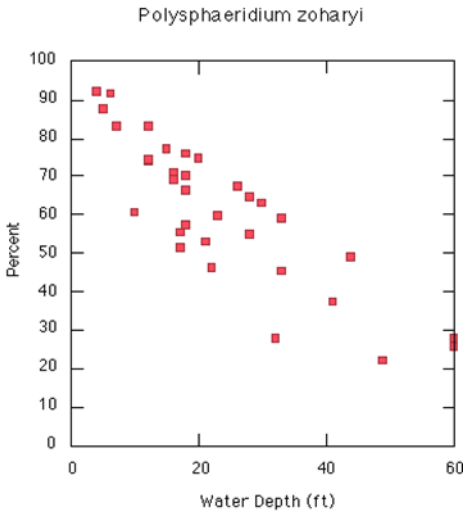

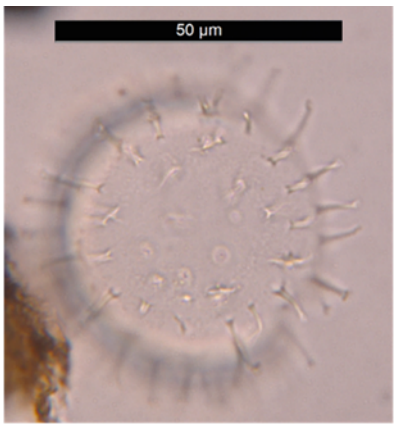

Figure 17. *Polysphaeridium zoharyi from Myrtle Grove 35m*

Figure 18. *Percentage composition of Polysphaeridium zoharyi (vertical axis) compared to water depth (horizontal axis). Taken from GOM, coastal areas offshore of eastern Mississippi and westernmost Alabama. From Edwards and Willard (2001).*

It was observed that *P. zoharyi* shows a higher abundance in sheltered areas behind barrier islands and a lower dominance in open passages between islands (Edwards and Willard, 2001). The abundance of *P. zoharyi* has however also been attributed to high salinity conditions (Morzadec-Kerfourn, 1983), with water depth as the controlling factor seen as unlikely. Edwards and Willard (2001) propose *P. zoharyi* as an indicator of abnormally low salinity, or a highly fluctuating salinity, with the possibility of the thecate stage of *P. zoharyi* migrating vertically to avoid contact with freshwater (Wall, 1977). The concentration of *Spiniferites* with small-mutated processes (Fig. 19), only present in Zone 1c, further supports a low salinity environment. The samples of Edwards and Willard (2001), collected at relatively shallow depths (up to 18 m), infer that it is likely the proximity to terrigenous freshwater input and the subsequent influence on salinity fluctuations and nutrient delivery that is the dominant control over *P.zoharyi* abundances. If salinity and freshwater input are indeed controlling the

abundance of *P. zoharyi* at the MG site, as in the study by Edwards and Willard (2001), this would not support the interpretation of a rising sea level and transgressive phase. However, as the presence of barrier islands is reported to increase the *P.zoharyi* abundance, a possible explanation is that the rising sea levels eroded barrier islands close to the MG site and therefore triggered the observed decline. It must be recognised that absolute dinocyst concentrations are low, therefore the reliability of larger interpretations using dinocysts data must be taken with caution. The expansion of salt marsh pioneer species such as *Chenopodiaceae* can be used as independent evidence of rapid sea level rise (Gonzalez and Dupont, 2009), within Zone 1 this links with the rapid decrease in BIT values.

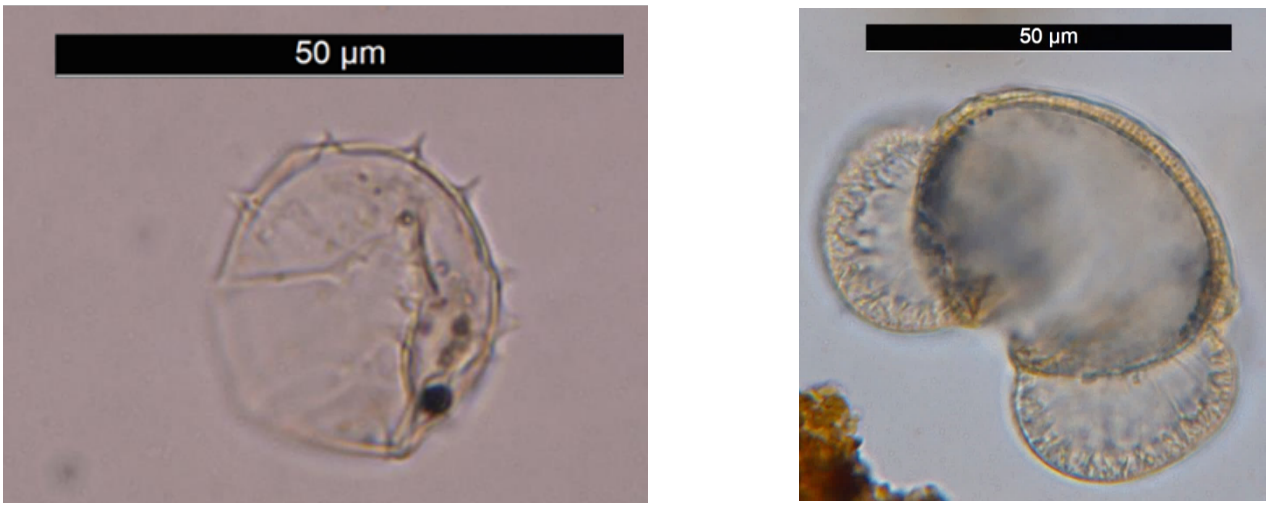

Figure. 19 *Left: Spiniferites featuring reduced processes due to low salinity Right: Pinus featuring air sacs to aid in wind dispersal*

5.2.2 Zone 1B - Zonal interpretation

Zone 1b can be interpreted as a small regression within the main transgressive phase. This observation is supported by biomarkers and $\delta^{13}C$ data (Fig. 14). The small decline in $\delta^{13}C$ values from of -24‰ to -25‰ indicates a shift to an increased input of terrestrial OM and a potential lowering of sea level (Dearing Crampton-Flood et al., 2018). A significant rise in BIT index values, from 0.2 to 0.6 by the end of 1b, and a significant decline in crenarchaeol and marine diols supports this interpretation (Fig. 14). A decrease in *Pinus* through this interval indicates a reduced dominance of wind-dispersed pollen in the assemblage and an increase of fluvially-derived pollen grains, particularly *Chenopodiaceae* (Fig. 16) and therefore a shoreline closer to the MG site. The C_{32} 1,15 proxy shows a gradual increase from 30 to 40 through Zone 1b indicating an increase in fresh water input. The increasing P_{aq} values from 0.45 to 0.63 indicate an appearance of submerged plants and therefore a shallower environment where they are

no longer ‘too-submerged’ to survive. The sharp decreases seen in both crenarchaeol and all marine diols (Fig. 14) infer changes in the marine realm, the most apparent conclusion is a regressive stage. However, evidence in the lithology that still infers a pro delta deposit and confident data on relative SL changes in the Holocene do not support the interpretation of a regression.

The age depth graph (Fig. 6) from $\delta^{14}C$ and luminescence dating from Bridgeman (2018) can be used to time known historical events to the trends presented in the MG data. A well-correlated event with the MG data is the 8.2 ka event. The 8.2 ka event is a recognised early Holocene, Century-scale cooling in the North Atlantic inferred from the Greenland Summit ice core records (Alley et al., 1997). It was triggered by a catastrophic release of meltwater from the North American proglacial lakes and the final collapse of the Laurentide ice sheet into the Labrador Sea (Barber et al., 1999; Clarke et al., 2003). Mississippi Delta peat records have been used by Törnqvist et al., (2004) to show that the relative SL rise was likely less than ~1.2 m, however the event is also associated with abrupt cooling of up to ~6°C in Greenland along with increased dryness and windiness in large parts of the Northern Hemisphere (Törnqvist et al., 2014). The significant increase in *Chenopodiceae* in Zone 1b may be related to this associated dryness as herbs often show an increase in the more arid conditions (Nannan et al., 2017) that may now exist further inland. The study by Delcourt et al., (1978) of a core taken on the Lower Mississippi Alluvial Valley, Southwest Tennessee, reveals that the Mississippi vegetation upstream was gradually replaced from alluvial swamp to marsh grasses, reflecting the warmth and dryness of the Holocene Climate Optimal occurring between 8.7-5 ka.

Enhanced Mississippi river discharge during the Holocene (Fig. 20) was inferred from peaks of Fe, Si and Al from a core taken in NW GOM (Tripsanas et al., 2013). The EMRD event dating between 8.6-8.9 ka (Zone 1b) has been related to the backflooding of the former Lake Agassiz, Canada and claimed by LoDico et al., (2006) to be diverted through the Mississippi river to the GOM. This interpretation has been further supported by the 8.5 ka EMRD event that finds it originated from the eastern Upper Mississippi (Tripsanas et al., 2013). It is likely that these flooding events caused the Mississippi river regime to change from braided to meandering in the Lower Mississippi Alluvial Valley at ~8.8 ka (Delcourt et al., 1978). Continued SL rise throughout this period may have however been the cause for a river regime change from braided to meandering. Zone 1b can therefore be interpreted as a lowering of relative SL, bringing the shoreline closer to MG, observed through the BIT index of 0.6 showing increased terrestrial input and the *Pinus* record inferring an increased fluvial input. The decline of dinocysts can be interpreted as salinity-driven, with an increased input of freshwater lessening ocean salinity further supporting the interpretation of an increased input of freshwater and nutrients from river systems. It is likely that in Zone 1b an increased freshwater input and thus biological evidence from upstream is released into the ocean at the MG site. A delta here is however not built as the RSL rise is higher than the sediment input into the system. The input of freshwater from the Mississippi river at the MG site may have however been restricted by

the former position of the river within the alluvial valley of the Mississippi. It is therefore proposed that a subsidiary river may have been redirected closer to the MG site.

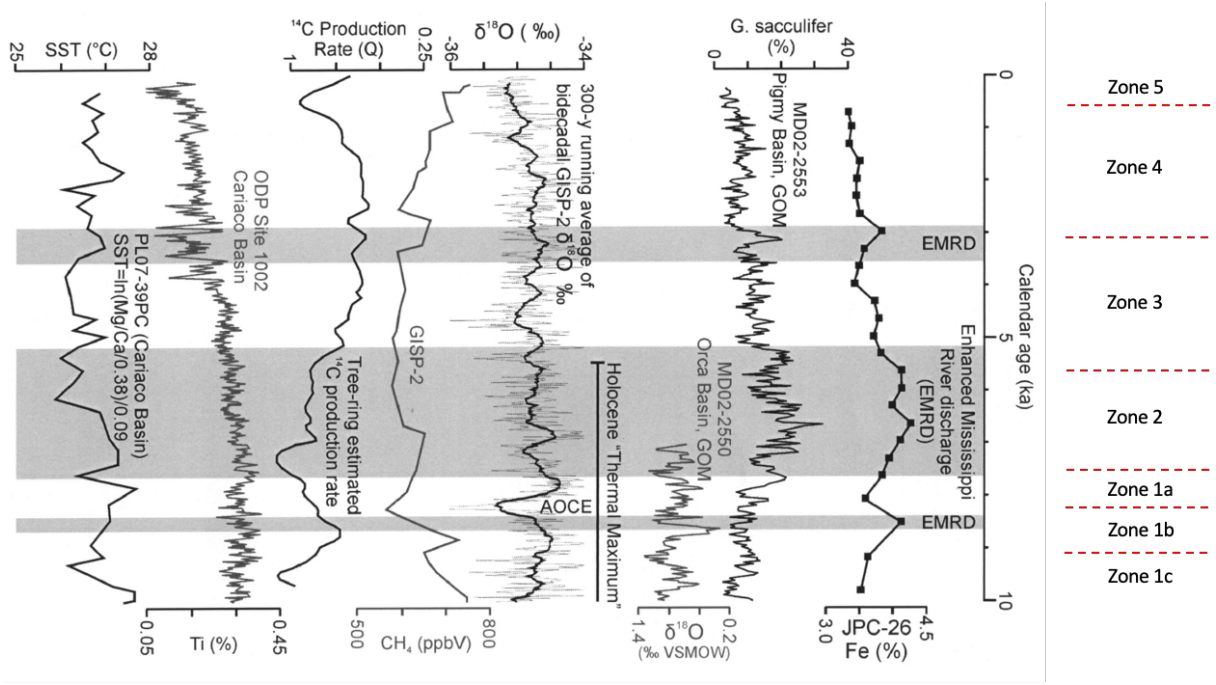

Figure 20. *EMRD events in the MRD altered (Tripsanas et al., 2013) to include zones for Myrtle Grove sample site and the correlation between zone 1b and Zone 2 with EMRD events.*

5.2.3 Zone 1A – Zonal interpretation

Zone 1a is within the clay lithology but has a sand layer at roughly 28.5 m (Fig. 7). Pro delta deposits of thick mud and silt can build up quickly due to a high sedimentation rate in a low-energy environment. The presence of a sandy layer suggests a high-energy phase or event occurring during the build-up of the pro delta deposit. The sand layer, located at ~28 m, correlates to the end of the transgressive phase capping Zone 1a of the MG samples. A second transgressive stage through Zone 1A can be inferred from the falling BIT index, from 0.6 to 0.3. Crenarchaeol and long-chain diols increase through Zone 1C, but to only a third of the values seen in Zone 1C (Fig. 14). A shoreline further away from the sample site can therefore be inferred with SL rise drowning the previous emergence of submerged vegetation seen in Zone 1b in the P_{aq} proxy indicated by value 0.3 (Fig. 15). The geochemical data infers a transgression and a coastline moving further away from the sample site. This is supported by a rise in *Pinus* in the pollen assemblage and a small increase in dinocysts concentration (50–300). However, as previously mentioned significant changes in SL are unlikely, as the trends

seen in the data most likely represent changes occurring upstream and the proximity of river discharge into the ocean relative to the MG sample site.

5.3 Zone 2 – Zonal interpretation

The lithology sequence from Bridgeman (2018) of homogenous silt and clays with few laminations still infers a pro delta deposit between 35–17 m, however biomarker and palynology data here can be used to explore changes further upstream and aid in reconstructing the proximity of the coastline to the MG site

Zone 2 is characterised by a steadily increasing BIT index, from 0.3 to 0.7, and C_{32} 1,15 indicating a transition from a marine environment to river-dominated terrestrial environment, with an increased input of terrestrial OM and freshening of the system. The absence of marine diols, C_{28} and C_{30} 1,14-diols, and low values of crenarchaeol (Fig. 14), coupled with known successions in the pollen assemblage and biomarker results, all support the interpretation of a regressive phase. This is also supported by low P_{aq} (0.2) and higher ACL (28.5) values indicating an increased contribution of arboreal vegetation (Fig. 15). In the pollen record herbs still dominate and typically show a local representation of the area compared to a regional wind-dispersed arboreal pollen taxa. The presence of *Lingulodinium machaerophonum*, although in low percentage, supports an increased fluvial presence, reflecting the BIT index and C_{32} 1,15 values.

Tsuga is a strictly northern taxa (Chmura and Liu, 1989) and is native to the Rocky Mountains and Northern America (Fig. 21). The presence of *Tsuga* and *Picea* show it is possible for these pollen grains to be transported ~2000 miles through the river system (Chruma and Liu, 1989). The increase in *Tsuga* within Zone 2 therefore can indicate an increased runoff from the West Coast Rocky Mountain catchment area and a flush of northern pollen grains into the sediment. This hypothesised intensified runoff may also explain the increase of terrestrial OM in the system by rivers transporting a higher sediment load at this time.

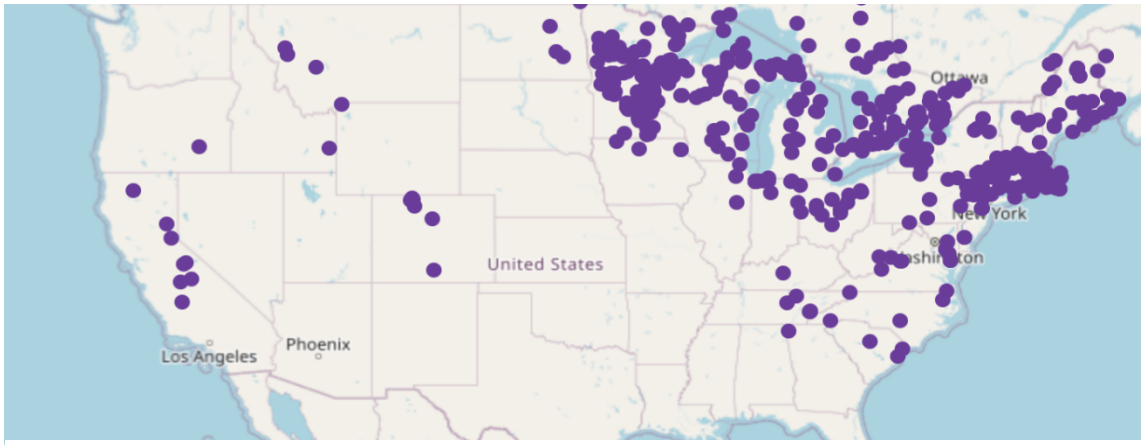

Figure 21. *Tsuga distribution of the last 10,000 years highlighting the northern growing environment. From Neotoma; Williams, Grimm et al. (2018)*

Although biomarker data and palynology support the interpretation of an increased input of terrestrial OM, likely from fluvial mechanisms, with marsh-like herb taxa beginning to colonise the environment, the lithology does not support this at the MG site. Within Zone 2 the lithology is still purely a low-energy pro delta environment. However, a proposed increase in drainage and sediment load may have transported evidence of environment change upstream to the sediment of the pro delta that Bridgeman (2018) interpreted from the subaqueous lithology. An EMRD event dating between 7.6-5.2 cal ka has been related to increased precipitation over central and eastern North America as the only process that could explain higher discharge (Tripsanas et al., 2013). From the age depth plot, this EMRD event occurred between ~27–17 m, matching with Zone 2 in the MG core. The findings of distinct peaks of Ti, K and smectite, abundant in Upper Mississippi, during this time indicate intense precipitation over the area of the Upper Mississippi Valley (Tripsanas et al., 2013). The orbitally-forced Holocene Climatic Optimum resulting in the northward migration of the Intertropical Convergence Zone (ITCZ) and strengthened monsoonal circulation is evident in the geological evidence from numerous lakes in central Mexico (Bradbury, 1989; Park et al., 2010). Poore et al., (2003) provides evidence of this phenomena in the GOM through the abundance of warm water foraminifera *Globigerinoides sacculifer,* as does Dwyer et al., (1996) through geological evidence of increased precipitation over Lake Ontario. The increase in terrigenous organic matter observed in Zone 2 could therefore be related to increased precipitation and river discharge over North America and the Upper Mississippi basins caused by the Holocene Climatic Optimum.

5.4 Zone 3 – Zonal interpretation

Within the lithology of Bridgeman (2018) there are significant changes throughout Zone 3. Between 20 and 10 m there is a change from the low-energy deposition of clay muds to high-energy deposition of silt and sand layers. The mm and cm thick laminations found above 17 m have been interpreted as delta front deposits and imply the river mouth has moved closer to

the sample site and a regression is indeed occurring (Bridgeman, (2018). Zone 3 is characterized by increasing C/N values, indicating a shift towards a more terrestrial source of the OM (Waterson and Canuel, 2008). Variation in IR, #rings$_{tetra}$ and C_{32} 1,15 values are small however the increase in BIT index values from 0.7 to 0.8 follows the previous trend of Zone 2 indicating increasing terrestrial matter into the system. The pollen record indicates an increasingly terrestrial environment with an increase in arboreal and wetland tree taxa. With the P_{aq} proxy, with low values of 0.2, and ACL values of 28.5 (Fig. 15), the biomarker data supports the trends in the pollen assemblage. The interpretation of this environment is subaqueous moving to terrestrial at the top of the zone. Palynology data shows the appearance and increase of acritarch's which also indicate a brackish environment with increased influence of freshwater (Stutz et al., 2010).

By 5.7 ka the rate of sea level rise had slowed enough to allow the sediment load of the Mississippi Delta to build out west of the sample site and build the Teche subdelta (Hijma et al., 2017) into water ~10 m deep (Fig. 3). The sub-deltas formed during periods of continuous relative SL rise, with the sedimentation supply to the coast and rate of deposition outpacing the SL rise (Gonzalez and Törnqvist, 2009). Hijma et al., (2017) dated peat beds of the Teche subdelta in three locations, recording near identical ages of 6 ka. Using the age depth plot (Fig. 6) it can be seen that a depth of 20 m in the MG core is at 6 ka. It can therefore be assumed that the increasing contribution of terrestrial OM to the site can be attributed to renewed sediment supply to the Mississippi Delta and a period of relatively stable SL. This is supported by the lithology and deposition of the mouth bar over the MG sample site. Mouth bar deposits form very rapidly as the delta progrades seaward indicating a regression and the delta building out into the ocean over the sample site. The deposition of the mouth bar occurred between 12-10 m (~3.4 ka) and coincides with the capture of increased sediment supply in the study area by the St. Bernard system (Fig. 3). This new sub-delta and additional sediment load allowed the mouth bar to build over the sample site (Bridgeman, 2018; Hijma et al., 2017).

5.5 Zone 4 – Zonal interpretation

From the lithology of alternating sand and silt it is clear that within Zone 4 the environment is subaerial and subject to overbank deposits (Bridgeman, 2018). The lithology of Zone 4 is the most dynamic, interpreted by Bridgeman (2018) as the presence of two sub-deltas, the St. Bernard (11.5–7.5 m) and the Plaquemines–Modern (6.5–1 m) separated by a marsh (7.5-6.5 m). An unconformity, identified through the presence of shells at the top of the marsh, is present at 6.3-6.4 m (Bridgeman, 2018). Biomarker and palynology will be hereby used to support and constrain the timing of these interpretations. High BIT index values of ~0.9 support primarily terrestrial OM being deposited with high C_{32} 1,15 values inferring a lack of marine influence Fig. 14).

Up to 7.5 m overbank deposits created a dynamic environment with flooding events distributing silt across the floodplain with low organic content (>15%) (Bridgeman, 2018). This

is supported by TOC values of 0.5. Low P_{aq} and higher ACL values reflect a vegetation change, with increasing emergent and terrestrial plants in the local area with wetland trees contributing to 15% of the assemblage and herbs of ~60%, supporting a floodplain environment of overbank flooding and backswamps. The change in lithology to peat at 7.5 m is interpreted as a marsh environment, this correlates with the peaks of TOC, $F_{C32\ 1,15}$ and the BIT index. Within this zone a high amount of organic matter accumulation, the sharp increase of TOC from 0.5 to 1.6, and CPI values from 1.2 to 3.5 further support a marsh interpretation (Fig. 15). In particular the sum of brGDGTs support an environment of anoxic conditions. brGDGTs are most abundant in the anoxic parts of peat (Peterse et al., 2011a). The increase of $F_{C32\ 1,15}$ indicates freshwater input to the sample site, with the environment flooded by freshwater overbank flows, it is likely the river is in close proximity. A freshwater influence is supported by a decrease in brackish water indicating acritarchs (Fig. 16).

The lithology change from peat to alternating silt and clay from 6.5 m to 1 m indicates the marsh was drowned and subsequently covered with overbank deposits. This is supported by the biomarker data with a decline in $F_{C32\ 1,15}$, TOC, the increase in $\#rings_{tetra}$ and the presence of shells in the lithology (Bridgeman, 2018). The steadily increasing P_{aq}, 0.25 to 0.65 and herb values up to 70% of the assemblage also support the interpretation of a drowned marsh becoming brackish and eventually turning it into bay environment signifying a transgression towards the MG site (Fig. 15).

The lithology of alternating sand and mud layers between 6.5–1 m shows that overbank flooding was renewed at the sample site with crevasse splays eroding much of the bay deposits (Bridgeman, 2018). This is likely the reason for biomarker and carbon data not showing evidence for a marine ingression like the previous transgression in Zone 1a-c. C/N ratios slightly decrease inferring a small increase in marine influence. TOC decreases due to a high-energy environment with fast deposition of coarser-grained sediment that does not allow for the accumulation of organic matter. The increase of herbs and particularly *Chenopodiaceae* shows an environment that is readily changing and that does not allow the growth and build-up of forested areas.

The alternating lithology and inferred depositional environments, overbank flooding and marsh in Zone 4 are the result of natural delta cycles that are internally forced, rather than influenced by SL and climate change. These delta cycles are present and easily noticeable in the MG sample site lithology, biomarker and palynology data and follow the trends highlighted by Twilley et al., (2016) in Fig. 3.

Zone 3 terminates with the deposition of the mouth bar (~3.4 ka) and therefore infers a prograding river mouth and shoreline regression. After 5.7 ka the St. Bernard system had captured more of the Mississippi River discharge and with the increased sediment supply it was able to build past the MG Sample site (Bridgeman, 2018). The coastline retreated as a result of continued progradation of the delta over the study site, replacing the marine pro delta environment with a floodplain environment with overbank flooding. This floodplain

environment formed as the channel periodically flooded, depositing coarse-grained sand proximal to the channel and silt and clay more distally. As the dominant river moved away from the MG site around 3.1 ka (8 m) sedimentation rates decreased, with flooding events depositing finer-grained mud rather than sand (Hijma et al., 2017). This lower-energy environment is likely a coastal marsh of a wetland. It can be seen at ~6-8 m in the data with peaks in TOC and the sum of brGDGTs indicating a low-energy anoxic environment. By 1.7 ka (~6 m) a delta lobe switch event occurred and the Lafourche delta began its progradation to the west (Coleman and Roberts, 1989). This deprived the St. Bernard delta of its sediment load leading to gradual inundation by marine waters and subsidence, noticed in the lithology as an unconformity and the presence of shells. The Plaquemines-Modern subdelta soon recaptured the Mississippi River as early as 1.4 ka, increasing sedimentation rates over the MG sample site and eroding any bay deposits via crevasse splays (Hijma et al., 2017), seen as sandy layer deposits in the upper 6m in the MG lithology. Between 5.3–0.9 m the landscape quickly aggraded with overbank floods continuing to be the main source of sediment supply to the environment suggesting the river was always close to the MG site.

5.6 Zone 5 – Zonal interpretation

The lithology from Bridgeman (2018) of peat infers a formation of a modern marsh. Zone 5 begins with a slight increase in $F_{C32\ 1,15}$ indicating the system is remaining fresh. An increase in the TOC suggests an increase of OM and decreasing sedimentation rate allowing for the build-up of OM in the sediment, this can infer a swamp-like environment. The upper half of Zone 5 (1 m) however shows opposing trends to the lower half (2-1 m) with salinity increasing, reflected in the IR and $F_{C32\ 1,15}$. However, it is known the environment changes and impacts within the upper 1 m are the result of human influence and the transition from the Holocene to the Anthropocene. With the creation of levees and locks, connections between tributaries and the Mississippi River have become detached, restricting sediment supply over the last century (Davis, 2000). With the creation of Mississippi River and tributaries levees around 1928, sediment supply was cut from the MG sample site (Bridgeman, 2018). The lack of overbank flooding previously supporting the subaerial nature of the delta resulted in the formation of the marsh seen today. An increase in the sum of brGDGTs and CPI in Zone 5 supports the lithological interpretation of a marsh environment with a higher pH and slow sedimentation rates. With the current lack of sediment, it is estimated that 35% of wetlands are vulnerable to submergence due to the slow rate of sediment accretion and opposing subsidence in the area (Jankowski et al., 2017).

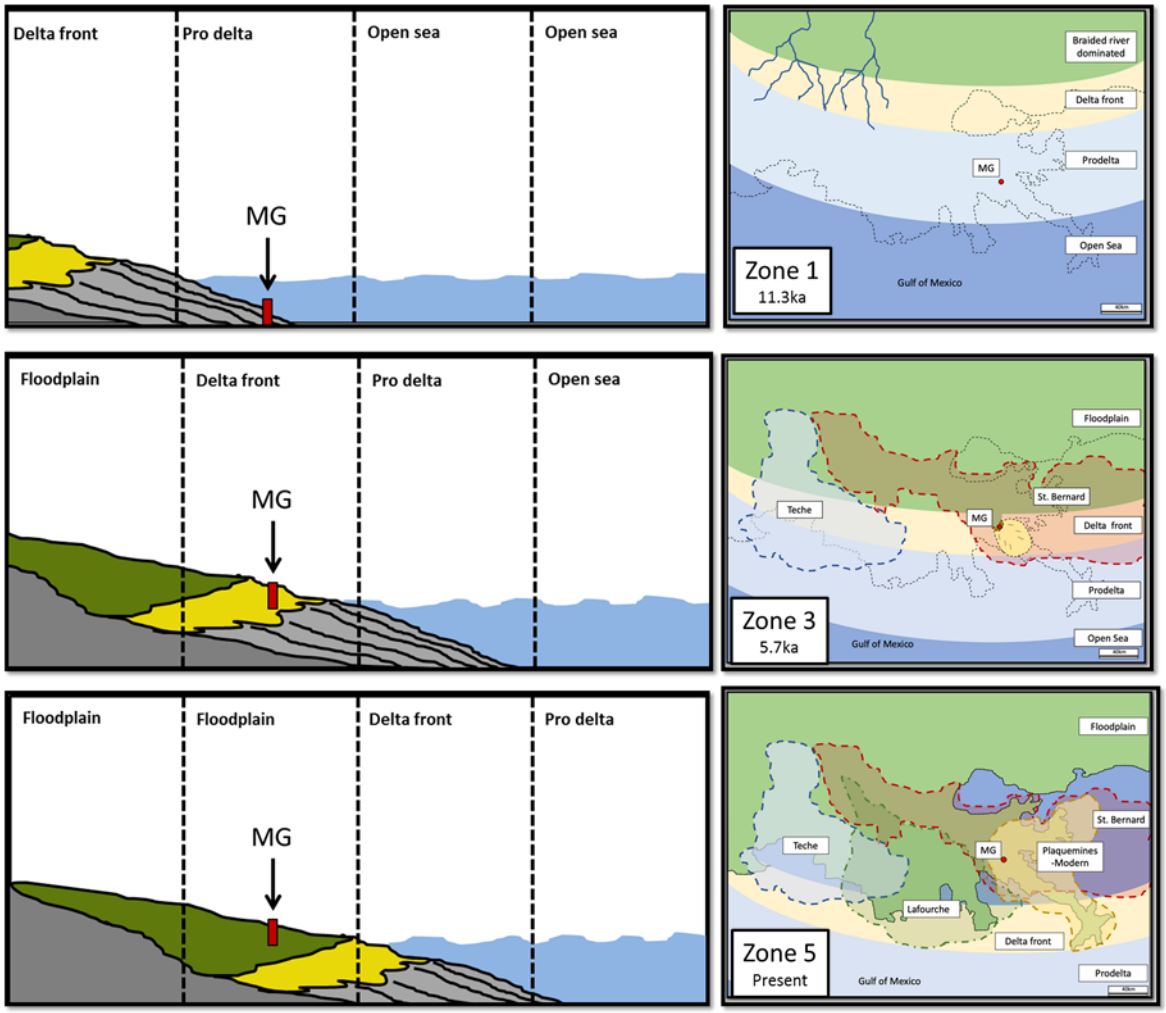

Figure 22. *Depositional environment changes through the Holocene. Green, yellow, light blue and blue depicting floodplain, delta front depositional area, pro delta depositional area and open sea, respectively. Present day outline of the MRD in dashed line is seen. MG is sample site Top: Reconstructed environment within Zone 1 depicting the pro delta deposits and inferred surrounding area. ~11 ka BP. Middle: Zone 3 with deposited delta front and prograding St. Bernard sub delta and retreating coastline ~5.7 ka BP. Bottom: Present day MRD coastline and sub deltas.*

5.7 Holocene carbon storage potential

The formation of coastal wetlands on the surface of deltaic deposits allows for continued high rates of carbon storage. Through the natural deltaic lifecycle, the wetland will eventually experience salinity increase as the river begins to avulse (Comeaux et al., 2021; Bianchi et al., 2013). The natural- and human- induced subsidence of the MRD can act as an aid in carbon storage. As areas of delta subside, OC is locked away in the sediment in long-term CO_2 storage.

TOC and CPI are indicators of efficient carbon storage (Fig. 23). TOC peaks at 7.5 and 1 m and CPI peaks at 9 m. Within these Zones the BIT Index, 0.9 at 7.5 m and 0.73 at 1 m, indicates a primarily terrestrial input of organic matter, the $F_{C32\ 1,15}$ at these depths is 77 and 65 respectively, indicating an environment with little marine influence. This is supported by C/N values of 7.5 and 19, respectively, indicating a terrestrial environment. Herbs contribute to 40 and 65% of the assemblage at depths 7.5 and 1 m respectively and wetland trees reach a high of 9.6 and 10.5%. Maximum peaks in brGDGTs occur at 7.5 m and 1 m reaching highs of 53 and 36 µg/g. From the MG data, 2 zones of optimum carbon storage (OCS) can be interpreted. OCS1 occurring between 2 and 0 m, ~500 ka - Present, and OCS2 between 10 and 5 m, 3.1–1.5 ka. The lithology from Bridgeman, (2018) shows that OCS1 occurs within modern peat deposits and can be interpreted as a modern marsh, whereas OCS2 occurs within laminated silt clay loam, silty clay and peat and can be interpreted as an inter-sub-delta marsh overlying overbank deposits. From the original interpreted lithology by Bridgeman, (2018) and the geochemical, palynological and bulk sediment properties, it can be confidently assumed that OCS1 and 2 occur in floodplain and/or wetland environments. The peaks in brGDGTs to 53 and 36 µg/g, in zones OCS1 and OCS2 respectively, can infer an anoxic environment (Peterse et al., 2011a). It is therefore likely that the peat lithology formed under ‘decomposition-limiting’ feedback conditions, the vegetation of wetland trees and herbs further supports this interpretation. It can be seen that the internal processes of delta lobe switching, and the accompanying floodplain and wetland environments, produce ideal environments for carbon storage, further highlighting their importance and need of protection. With the identification of environments with high carbon storage potential, future engineering of the MRD can be influenced. Current work on the Mississippi/Atchafalaya River delta involves the use of sustainable environmental engineering, using the natural river’s ability to build land, and diverting it to basins in need (LACPRA, 2017; Day et al., 2018). Louisiana’s management plan (LACPRA, 2017) recognises the importance of CO_2 sequestration in coastal wetlands, with the study of Shields et al., (2017) showing carbon storage should be a real and quantifiable benefit of delta land-building processes.

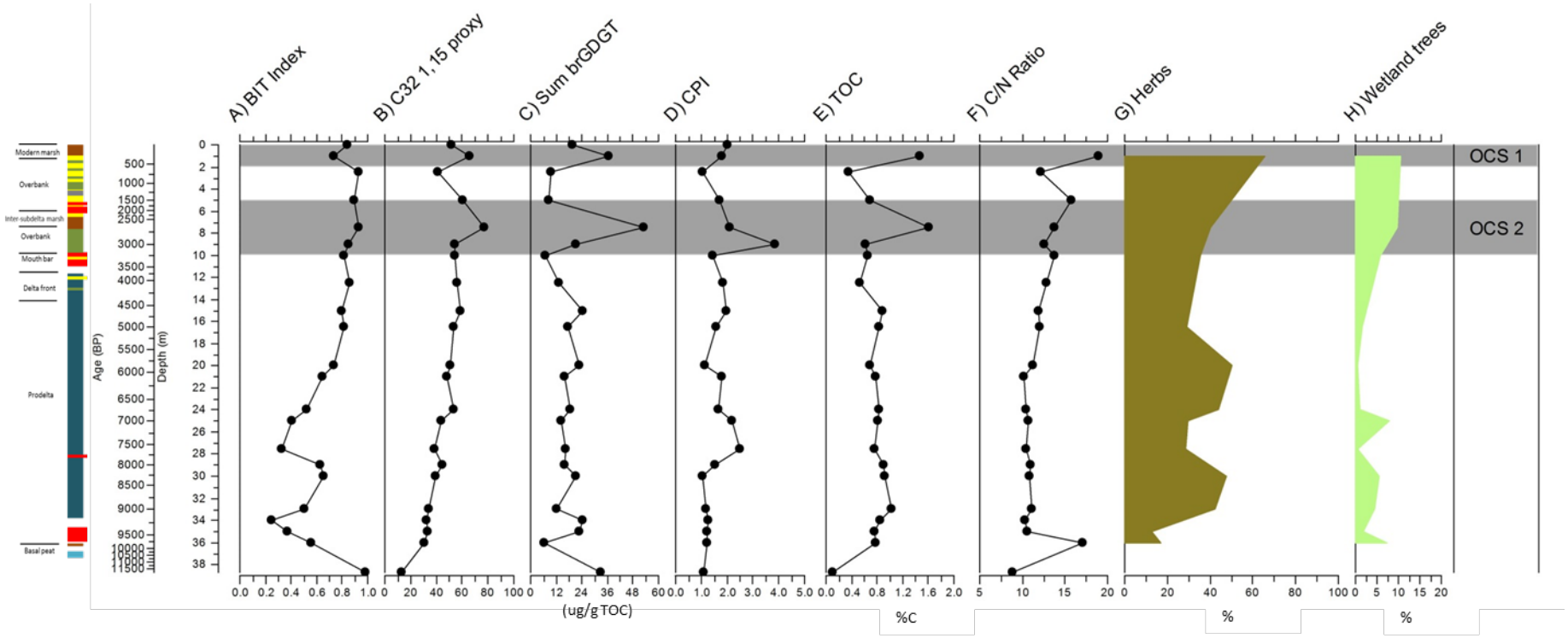

Figure 23. *Lipid biomarker, bulk sediment and palynological proxies interpreting a wetland environment and optimum carbon storage zones (OCS). A) BIT Index, B) C32 1,15, C) brGDGTs, D) n-alkane CPI, E) TOC, F) C/N ratio, G) Herbs, H) Wetland trees. Interpreted zones of OCS displayed in grey.*

6. Conclusion

Bulk sediment, geochemical and palynology analyses of a 38.7 m core provide further insight into the depositional environment evolution of the Myrtle Grove superstation site. Zones have been created using the lithology and trends seen in the data. The initial transgression in Zone 1 is highlighted by a rapidly decreasing BIT Index and increasing $\delta^{13}C$ values within prodelta deposits between 38.7 and 28 m. Zone 2 contains a rapidly increasing BIT index and freshening of the system seen through the $F_{C32\ 1,15}$,however still within the pro-delta deposit it has been interpreted as increased fluvial input into the coastal marine realm. The lithology in Zone 3 transitions from marine pro delta towards a more terrestrial environment with the deposition of a delta mouth bar. This is reflected in the C/N ratio, BIT Index and appearance of brackish water acritarchs. Zone 4 is a predominantly terrestrial environment, inferred by floodplain overbank and peat marsh deposits. This is supported by high BIT Index, $F_{C32\ 1,15}$ and herbaceous pollen. Zone 4 highlights the influence that delta lobe switching has on the depositional environment, with the St. Bernard, Lafouche and Plaquesmines-Modern sub-deltas redirecting and redistributing water and sediment across the Mississippi Delta landscape. Within Zone 5 the lithology changes back to a marsh environment. Within this Zone human influences such as damming are shown in the environments, reducing sediment load and therefore terrestrial signal to the study site. Bulk sediment analysis showing TOC and lipid biomarker analysis of n-alkanes CPI index highlights areas where carbon is best sequestered. Two zones of optimal carbon storage have been interpreted, with the lithology, palynology, BIT Index and $F_{C32\ 1,15}$ inferring a wetland environment. This is supported by current literature of the carbon storage potential of wetlands in the coastal environment. This research further highlights the importance for wetland protection and restoration and can be used to aid the engineering work on the MRD.

8. References:

Adam, P., (1990). Saltmarsh Ecology. Cambridge University Press, Cambridge, p. 461.

Aharon P., (2003) Meltwater flooding events in the Gulf of Mexico revisited: Implications for rapid climate changes during the last deglaciation. Paleoceanography 18(4): 1079.

Alley, R.B., Mayewski, P.A., Sowers, T., Stuiver, M., Taylor, K.C. and Clark, P.U., (1997). Holocene climatic instability: A prominent, widespread event 8200 yr ago. Geology, 25(6), pp.483-486.

Allison, M., Yuill, B., Törnqvist, T., Amelung, F., Dixon, T.H., Erkens, G., Stuurman, R., Jones, C., Milne, G., Steckler, M., Syvitski, J., and July, P.T., (2016), Global Risks and Research Priorities for Coastal Subsidence: Eos, Transactions American Geophysical Union, no. 97, p. 22–27.

Bard, E., Hamelin, B., Arnold, M., Montaggioni, L., Cabioch, G., Faure, G., & Rougerie, F. (1996). Deglacial sea-level record from Tahiti corals and the timing of global meltwater discharge. Nature, 382(6588), 241-244.

Barber, D.C., Dyke, A., Hillaire-Marcel, C., Jennings, A.E., Andrews, J.T., Kerwin, M.W., Bilodeau, G., McNeely, R., Southon, J., Morehead, M.D. and Gagnon, J.M., (1999). Forcing of the cold event of 8,200 years ago by catastrophic drainage of Laurentide lakes. Nature, 400(6742), pp.344-348.

Batker, D., De La Torre, I., Costanza, R., Swedeen, P., Day, J., Boumans, R. and Bagstad, K., (2010). Gaining ground: wetlands, hurricanes, and the economy: the value of restoring the Mississippi River Delta. Envtl. L. Rep. News & Analysis, 40, p.11106.

Bentley Sr, S. J., Blum, M. D., Maloney, J., Pond, L., & Paulsell, R., (2016). The Mississippi River source-to-sink system: Perspectives on tectonic, climatic, and anthropogenic influences, Miocene to Anthropocene. Earth-Science Reviews, 153, 139-174.

Bianchi, T.S., Allison, M.A., Zhao, J., Li, X., Comeaux, R.S., Feagin, R.A. and Kulawardhana, R.W., (2013). Historical reconstruction of mangrove expansion in the Gulf of Mexico: linking climate change with carbon sequestration in coastal wetlands. Estuarine, Coastal and Shelf Science, 119, pp.7-16.

Blum, M.D. and Törnqvist, T.E., (2000) Fluvial responses to climate and sea-level change: A review and look forward. Sedimentology 47: 2–48.

Blum, M.D., Roberts, H.H., (2009). Drowning of the Mississippi Delta due to insufficient sediment supply and global sea-level rise. Nat. Geosci. 2:488–91

Blum, M.D. and Roberts, H.H., (2012). The Mississippi delta region: past, present, and future. Annual Review of Earth and Planetary Sciences, 40, pp.655-683.

Boyd, J.L., 2016. Global and regional assessment of Neogene climate and palaeoceanography using dinoflagellate cysts (Doctoral dissertation, University of Leeds).

Bradbury, J.P., (1989), Late Quaternary lacustrine paleoenvironments in the Cuenca de Mexico: Quaternary Science Reviews, 8, 75-100

Brassell, S.C., Eglinton, G., Marlowe, I.T., Pflaumann, U. and Sarnthein, M., 1986. Molecular stratigraphy: a new tool for climatic assessment. *Nature*, *320*(6058), pp.129-133.

Brugam, R.B., and Munoz SE (2018) A 1600-year record of human impacts on a floodplain lake in the Mississippi River Valley. Journal of Paleolimnology 60(3): 445–460.

Bridgeman, J.G., 2018. Understanding Mississippi Delta subsidence through stratigraphic and geotechnical analysis of a continuous Holocene core at a subsidence superstation (Doctoral dissertation, Tulane University School of Science and Engineering).

Chmura, G.L. and Liu, K.B., (1990). Pollen in the lower Mississippi River. Review of Palaeobotany and Palynology, 64(1-4), pp.253-261.

Church JA, White NJ, Aarup T, Wilson WS, Woodworth PL, et al. 2008. Understanding global sea levels: past, present and future. Sustain. Sci. 3:9–22

Clark, P.U., Shakun, J.D., Marcott, S.A., Mix, A.C., Eby, M., Kulp, S., Levermann, A., Milne, G.A., Pfister, P.L., Santer, B.D. and Schrag, D.P., (2016). Consequences of twenty-first-century policy for multi-millennial climate and sea-level change. Nature climate change, 6(4), pp.360-369.

Clarke, G., D. Leverington, J. Teller, and A. Dyke., (2003), Superlakes, megafloods, and abrupt climate change, Science, 301, 922– 923.

Clymo, R. S. (1964). The origin of acidity in Sphagnum bogs. The Bryologist, 67(4), 427-431.Coleman, J.M. and Roberts, H.H., (1989). Deltaic coastal wetlands. In Coastal Lowlands (pp. 1-24). Springer, Dordrecht.

Comeaux, R. S., Allison, M. A., and Bianchi, T. S., (2012). Mangrove expansion in the Gulf of Mexico with climate change: Implications for wetland health and resistance to rising sea levels. Estuarine, Coastal and Shelf Science, 96, 81-95.

Couvillion, B.R., Barras, J.A., Steyer, G.D., Sleavin, W., Fischer, M., Beck, H., Trahan, N., Griffin, B. and Heckman, D., (2011). Land area change in coastal Louisiana from 1932 to 2010. Sci. Investig. Map 3164, US Geol. Surv., Washington, DC

Couvillion, B.R., Beck, H. (2013). Marsh collapse thresholds for coastal Louisiana estimated using elevation and vegetation data. J. Coast. Res., 63, pp. 58-67

Cox, R.T., Lumsden, D.N. and Van Arsdale, R.B., (2014) Possible relict meanders of the Pliocene Mississippi River and their implications. The Journal of Geology 122(5): 609–622.

Cranwell PA (1973) Chain-length distribution of n-alkanes from lake sediments in relation to post-glacial environmental change. Freshw Biol 3:259–265

Dang, X., Ding, W., Yang, H., Pancost, R.D., Naafs, B.D.A., Xue, J., Lin, X., Lu, J. and Xie, S., (2018). Different temperature dependence of the bacterial brGDGT isomers in 35 Chinese lake sediments compared to that in soils. Organic Geochemistry, 119, pp.72-79.

Day, J.W., Jr, Boesch D.F., Clairain E.J., Kemp G.P., Laska S.B., Mitsch W.J., Orth K, Mashriqui H, Reed D.R., Shabman L, Simenstad C.A., Streever B.J., Twilley R.R., Watson C.C., Wells J.T., Whigham D.F., (2007) Restoration of the Mississippi Delta: lessons From hurricanes Katrina and Rita. Science 315:1679–1684

Day, J.W., Lane, R.R., D'Elia, C.F., Wiegman, A.R., Rutherford, J.S., Shaffer, G.P., Brantley, C.G. and Paul Kemp, G., (2018). Large infrequently operated river diversions for Mississippi delta restoration. In Mississippi delta restoration (pp. 113-133). Springer, Cham.

De Bar M. W., Dorhout D. J. C., Hopmans E. C., Sinninghe Damste´ J. S. and Schouten S. (2016) Constraints on the application of long chain diol proxies in the Iberian Atlantic margin. Org. Geochem. 101, 184–195.

De Jonge, C., Hopmans, E.C., Zell, C.I., Kim, J.H., Schouten, S. and Damsté, J.S.S., (2014a). Occurrence and abundance of 6-methyl branched glycerol dialkyl glycerol tetraethers in soils: Implications for palaeoclimate reconstruction. Geochimica et Cosmochimica Acta, 141, pp.97-112.

De Jonge, C., Stadnitskaia, A., Hopmans, E.C., Cherkashov, G., Fedotov, A., Sin-ninghe Damsté, J.S., (2014b). In situ produced branched glycerol dialkyl glycerol tetraethers in suspended particulate matter from the Yenisei River, Eastern Siberia. Geochim. Cosmochim. Acta125, 476–491.

De Jonge, C., Stadnitskaia, A., Hopmans, E.C., Cherkashov, G., Fedotov, A., Streletskaya, I.D., Vasiliev, A.A., Sinninghe Damsté, J.S., (2015). Drastic changes in the distribution of branched tetraether lipids in suspended matter and sediments from the Yenisei River and Kara Sea (Siberia): implications for the use of brGDGT-based proxies in coastal marine sediments. Geochim. Cosmochim. Acta165, 200–225.

de Vernal, A., (2009). Marine palynology and its use for studying nearshore environments. In IOP Conference Series: Earth and Environmental Science Vol. 5, No. 1, p. 012002.

Delcourt, P.A. and Delcourt, H.R., (1996). Quaternary paleoecology of the Lower Mississippi Valley. Engineering Geology, 45(1-4), pp.219-242.

Edwards, L.E, Willard, D.A., (2001). Dinoflagellate Cysts and Pollen from Sediment Samples, Mississippi Sound and Gulf of Mexico. Stratigraphic and Paleontologic Studies of the Neogene and Quaternary Sediments in Southern Jackson. County, Mississippi. USGS. Chapter D 01-415

Eglinton, G. and Hamilton, R.J., 1967. Leaf Epicuticular Waxes: The waxy outer surfaces of most plants display a wide diversity of fine structure and chemical constituents. *Science*, *156*(3780), pp.1322-1335.

Emerson, S., & Hedges, J. I. (1988). Processes controlling the organic carbon content of open ocean sediments. Paleoceanography, 3(5), 621-634.English J.M., and Johnston S.T., (2004) The Laramide orogeny: What were the driving forces? International Geology Review 46(9): 833–838.

Ficken, K. J., Li, B., Swain, D. L., & Eglinton, G. (2000). An n-alkane proxy for the sedimentary input of submerged/floating freshwater aquatic macrophytes. Organic geochemistry, 31(7-8), 745-749.

Fisk H.N., (1944). Geological Investigation of the Alluvial Valley of the Lower Mississippi River. Vicksburg, MS: US Army Corps Eng.

Fulton R.J., and Prest V.K., (1987) Introduction: The Laurentide ice sheet and its significance. Géographie physique et Quaternaire 41(2): 181–186.

Gagliano S.M., Van Beek J.L., (1975) An approach to multiuse management in the Mississippi delta system, pp 223–238. In: Broussard MS (ed) Deltas, models for exploration. Houston Geological Society, Texas, 555 pp

Galloway W.E., (2008). Depositional evolution of the Gulf of Mexico sedimentary basin. In Sedimentary Basins of the World, ed. AD Miall, 5:505–49. Amsterdam: Elsevier

Gebühu C, G., Sheward R.M., Herrle, J.O., Bollmann, J., (2021). Strain-specific morphological response of the dominant calcifying phytoplankton species to salinity change. PLoS ONE 16(2)

Gosselink J.G., Coleman J.M., Stewart R.E., (1998) Coastal Louisiana. In: Mac MJ, Opler PA, Haecker CEP, Doran PD (eds) Status and trends of the nation's biological resources. US Geol. Surv., Reston, pp 385–436

Heusser, L.E., and Balsam, W.L., (1977), Pollen distribution in the northeast Pacific Ocean: Quaternary Research, v. 7, p. 45-62.

Hijma, M. P., Shen, Z., Törnqvist, T. E., & Mauz, B. (2017). Late Holocene evolution of a coupled, mud-dominated delta plain–chenier plain system, coastal Louisiana, USA. Earth Surface Dynamics, 5(4), 689-710.

Hoffmann, B., Kahmen, A., Cernusak, L.A., Arndt, S.K. and Sachse, D., (2013). Abundance and distribution of leaf wax n-alkanes in leaves of Acacia and Eucalyptus trees along a strong humidity gradient in northern Australia. Organic Geochemistry, 62, pp.62-67.

Hopmans, E.C., Weijers, J.W.H., Schefuss, E., Herfort, L., Sinninghe Damsté, J.S., Schouten, S., (2004). A novel proxy for terrestrial organic matter in sediments based on branched and isoprenoid tetraether lipids. Earth and Planetary Science Letters 24, 107–116

Juggins. S. (2007). C2 Version 1.5 User guide. Software for ecological and palaeoecological data analysis and visualisation. Newcastle University, Newcastle upon Tyne, UK. 73pp.

Knox J.C., (2007). The Mississippi River system. In Large Rivers: Geomorphology and Management, pp. 145–81. London:Wiley

LACPRA Louisiana's Comprehensive Master Plan for a Sustainable Coast (Coastal Protection and Restoration Authority of Louisiana). (2017).

Lattaud, J., Kim, J.H., De Jonge, C., Zell, C., Damsté, J.S.S. and Schouten, S., (2017). The C32 alkane-1, 15-diol as a tracer for riverine input in coastal seas. Geochimica et Cosmochimica Acta, 202, pp.146-158.

Limoges, A., Kielt, J.F., Radi, T., Ruíz-Fernandez, A.C. and de Vernal, A., 2010. Dinoflagellate cyst distribution in surface sediments along the south-western Mexican coast (14.76 N to 24.75 N). Marine Micropaleontology, 76(3-4), pp.104-123.

Limoges, A., Londeix, L. and de Vernal, A., (2013). Organic-walled dinoflagellate cyst distribution in the Gulf of Mexico. Marine Micropaleontology, 102, pp.51-68.

LoDico, J.M., Flower, B.P., and Quinn, T.M., (2006), Subcentennial-scale climatic and hydrologie variability in the Gulf of Mexico during the early Holocene: Paleoceanography, v. 21, PA3015

MacDicken, K. G. (2015). Global forest resources assessment 2015: what, why and how?. Forest Ecology and Management, 352, 3-8.

MacDonald, K.B. and Barbour, M.G., (1974). Beach and salt marsh vegetation of the North American Pacific coast. Ecology of halophytes, pp.175-233.

McAndrews, J. H., (1988). Human disturbance of North American forests and grasslands: The fossil pollen record. In: Huntley, B. & Webb, T. Ill (eds.) Vegetation History, Kluwer Academic Publishers, pp. 673-697.

McIntyre, A. (1967). Modern coccolithophoridea of the Atlantic ocean – I. Placoliths and cyroliths. Deep Sea Research and Oceanographic Abstracts. 14 (5): 561-597

Mcleod, E., Chmura, G.L., Bouillon, S., Salm, R., Björk, M., Duarte, C.M., Lovelock, C.E., Schlesinger, W.H. and Silliman, B.R., (2011). A blueprint for blue carbon: toward an improved understanding of the role of vegetated coastal habitats in sequestering CO2. Frontiers in Ecology and the Environment, 9(10), pp.552-560.

Meade RH, Moody JA. (2010). Causes for the decline of suspended-sediment discharge in the Mississippi River system, 1940–2007. Hydrol. Process. 24:35–49

Middelburg, J. J., Nieuwenhuize, J., Lubberts, R. K., & Van de Plassche, O. (1997). Organic carbon isotope systematics of coastal marshes. Estuarine, Coastal and Shelf Science, 45(5), 681-687.

Morton, R. a., and Bernier, J.C., 2010, Recent Subsidence-Rate Reductions in the Mississippi Delta and Their Geological Implications: Journal of Coastal Research, v. 26, no. 3, p. 555–561

Morzadec-Kerfourn, M.-T., (1983), Intérêt des kystes de dinoflagellés pour l'établissement de reconstitution paléogéographique: exemple du Golf de Gabès (Tunisie): Cahiers de Micropaléontologie v. v, p. 15-22.

Mudie, P.J., (1982), Pollen distribution in recent marine sediments, eastern Canada: Canadian Journal of Earth Sciences, v. 19, p. 729- 747.

Lattaud, J., Balzano, S., van der Meer, M.T., Villanueva, L., Hopmans, E.C., Damsté, J.S.S. and Schouten, S., (2021). Sources and seasonality of long-chain diols in a temperate lake (Lake Geneva). Organic Geochemistry, 156, p.104223.

Li, N., Sack, D., Gao, G., Liu, L., Li, D., Yang, X., ... & Leng, C. (2018). Holocene Artemisia-Chenopodiaceae-dominated grassland in North China: real or imaginary?. The Holocene, 28(5), 834-841.Park, J., Byrne, R., Böhnel, H., Garza, R.M., and Conserva, M., (2010), Holocene climate change and human impact, central Mexico: A record based on maar lake pollen and sediment chemistry: Quaternary Science Reviews, v. 29, p. 618-632.

Peterse, F., Kim, J.H., Schouten, S., Kristensen, D.K., Koç, N., Sinninghe Damsté, J.S., (2009). Constraints on the application of the MBT/CBT palaeothermometer at high latitude environments (Svalbard, Norway). Org. Geochem.40, 692–699.

Poore, R.Z., Dowsett, H.J., Verado, S., and Quinn, T.M., (2003). Millenial – to century – scale variability in Gulf of Mexico Holocene climate records; Paleoceanography, v.18, no.2, p 1048

Potter-McIntyre S.L., Breeden J.R. and Malone D.H., (2018) A Maastrichtian birth of the ancestral Mississippi river system: Evidence from the U-Pb detrital zircon geochronology of the McNairy Sandstone, Illinois, USA. Cretaceous Research 91: 71–79.

Poumot, C., (1989). Palynological evidence for eustatic events in the tropical Neogene. Bulletin des Centres de Recherches Exploration–Production Elf Aquitaine 13, 437–453.

Rampen S.W., Schouten S., Koning E., Brummer G.-J.A. and Sinninghe Damste´ J. S. (2008) A 90 kyr upwelling record from the northwestern Indian Ocean using a novel long-chain diol index. Earth Planet. Sci. Lett. 276, 207–213.

Rampen S. W., Schouten S., Wakeham S. G. and Sinninghe Damste´ J. S. (2007) Seasonal and spatial variation in the sources and fluxes of long chain diols and mid-chain hydroxyl methyl alkanoates in the Arabian Sea. Org. Geochem. 38, 165– 179.

Rampen S.W., Shouten, S. and Sinninghe Damste´ J.S. (2011) Occurrence of long chain 1,14 diols in Apedinella radians. Org. Geochem. 42, 572–574.

Rampen, S. W., Willmott, V., Kim, J. H., Rodrigo-Gámiz, M., Uliana, E., Mollenhauer, G., ... & Schouten, S. (2014). Evaluation of long chain 1, 14-alkyl diols in marine sediments as indicators for upwelling and temperature. Organic Geochemistry, 76, 39-47.

Rampen S. W., Willmott V., Kim J.-H., Uliana E., Mollenhauer G., Schefuß E., Sinninghe Damste´ J. S. and Schouten S. (2012) Long chain 1,13- and 1,15-diols as a potential proxy for palaeotemperature reconstruction. Geochim. Cosmochim. Acta 84, 204–216.

Ranwell, D.S., (1972). Ecology of Salt Marshes and Sand Dunes. Chapman and Hall, 258 p.

Rittenour T.M., Blum M.D., and Goble R.J., (2007) Fluvial evolution of the lower Mississippi River valley during the last 100 k.y. glacial cycle; response to glaciation and sea-level change. Geological Society of America Bulletin 119(5–6): 586–608

Rosell-Melé A., McClymont E.L., (2007) Chapter eleven biomarkers as paleoceanographic proxies. Developments in marine geology. Volume 1, 441-490.

Rochon, A., Vernal, A.D., Turon, J.L., Matthiessen, J. and Head, M.J., 1999. Distribution of recent dinoflagellate cysts in surface sediments from the North Atlantic Ocean and adjacent seas in relation to sea-surface parameters. American Association of Stratigraphic Palynologists Contribution Series, 35, pp.1-146.

Russell, C., Waters, C.N., Himson, S., Holmes, R., Burns, A., Zalasiewicz, J., Williams, M. (2021). Geological evolution of the Mississippi River into the Anthropocene. The Anthropocene Review. 1-26

Schouten, S., Hopmans, E.C., and Damsté, J.S.S., (2013). The organic geochemistry of glycerol dialkyl glycerol tetraether lipids: A review. Organic geochemistry, 54, pp.19-61.

Shields, M.R., Bianchi, T.S., Mohrig, D., Hutchings, J.A., Kenney, W.F., Kolker, A.S. and Curtis, J.H., (2017). Carbon storage in the Mississippi River delta enhanced by environmental engineering. Nature Geoscience, 10(11), pp.846-851.

Sinninghe Damste´ J. S., Rijpstra W. I. C., Hopmans E. C., Weijers J. W. H., Foesel B. U., Overmann J. and Dedysh S. N. (2011) 13,16-Dimethyl octacosanedioic acid (iso-diabolic acid),

a common membrane-spanning lipid of Acidobacteria subdivisions 1 and 3. Appl. Environ. Microbiol. 77, 4147–4154.

Sinninghe Damste´ J. S. (2016) Spatial heterogeneity of sources of branched tetraethers in shelf systems: The geochemistry of tetraethers in the Berau River delta (Kalimantan, Indonesia) Geochimica et Cosmochimica Acta 186, 13–31

Sinninghe Damste´ J.S., Hopmans E.C., Schouten S., van Duin A.C.T. and Geenevasen J.A.J. (2002). Crenarchaeol: the characteristic core glycerol dibiphytanyl glycerol tetraether membrane lipid of cosmopolitan pelagic crenarchaeota. J. Lipid Res. 43, 1641–1651.

Stutz, S., Borel, C.M., Fontana, S.L., Del Puerto, L., Inda, H., García-Rodriguez, F. and Tonello, M.S., (2010). Late Holocene climate and environment of the SE Pampa grasslands, Argentina, inferred from biological indicators in shallow, freshwater Lake Nahuel Rucá. Journal of Paleolimnology, 44(3), pp.761-775.

Syvitski, J.P.M., Milliman, J.D., (2007). Geology, geography, and humans battle for dominance over the delivery of fluvial sediment to the coastal ocean. J. Geol. 115:1–19

Temmink, R. J., Lamers, L. P., Angelini, C., Bouma, T. J., Fritz, C., van de Koppel, J., ... & van der Heide, T. (2022). Recovering wetland biogeomorphic feedbacks to restore the world's biotic carbon hotspots. Science, 376(6593), eabn1479.

Tripsanas, E.K., Karageorgis, A.P., Panagiotopoulos, I.P., Koutsopoulou, E., Kanellopoulos, T.D., Bryant, W.R. and Slowey, N.C., (2013). Paleoenvironmental and paleoclimatic implications of enhanced Holocene discharge from the Mississippi river based on the sedimentology and geochemistry of a deep core (jpc-26) from the gulf of Mexico enhanced Mississippi river discharge. palaios, 28(9), pp.623-636.

Törnqvist, T.E., González, J.L., Newsom, L.A., Van der Borg, K., De Jong, A.F. and Kurnik, C.W., 2004. Deciphering Holocene sea-level history on the US Gulf Coast: A high-resolution record from the Mississippi Delta. Geological Society of America Bulletin, 116(7-8), pp.1026-1039.

Twilley, R.R., Bentley, S.J., Chen, Q., Edmonds, D.A., Hagen, S.C., Lam, N.S.N., Willson, C.S., Xu, K., Braud, D., Hampton Peele, R. and McCall, A., (2016). Co-evolution of wetland landscapes, flooding, and human settlement in the Mississippi River Delta Plain. Sustainability science, 11(4), pp.711-731.

Twilley, R.R., Bentley, S.J., Chen, Q., Edmonds, D.A., Hagen, S.C., Lam, N.S.N., Willson, C.S., Xu, K., Braud, D., Hampton Peele, R. and McCall, A., (2016). Co-evolution of wetland landscapes, flooding, and human settlement in the Mississippi River Delta Plain. Sustainability science, 11(4), pp.711-731.

Tyson, R.V. (1995) Sedimentary Organic Matter: Organic Facies and Palynofacies. Chapman & Hall, London, 615p.

Versteegh G. J. M., Bosch H. J. and de Leeuw J. W. (1997) Potential palaeoenvironmental information of C24 to C36 midchain diols, keto-ols and mid-chain hydroxy fatty acids; A critical review. Org. Geochem. 27, 1–13.

Volkman J. K., Barrett S. M. and Blackburn S. I. (1999) Eustigmatophyte microalgae are potential sources of C29 sterols, C22–C28 n-alcohols and C28–C32 n-alkyl diols in freshwater environments. Org. Geochem. 30, 307–318.

Wall, D., Dale, B., 1969. The "Hystrichosphaerid" resting spore of the dinoflagellate Pyrodinium bahamense. Journal of Phycology 5, 140–149.

Wang, J., Axia, E., Xu, Y., Wang, G., Zhou, L., Jia, Y., Chen, Z. and Li, J., (2018). Temperature effect on abundance and distribution of leaf wax n-alkanes across a temperature gradient along the 400 mm isohyet in China. Organic Geochemistry, 120, pp.31-41.

Waterson, E.J. and Canuel, E.A., (2008). Sources of sedimentary organic matter in the Mississippi River and adjacent Gulf of Mexico as revealed by lipid biomarker and $\delta^{13}C$ TOC analyses. Organic Geochemistry, 39(4), pp.422-439.

Wickert, A.D., Mitrovica, J.X., Williams, C. and Anderson, R.S., (2013). Gradual demise of a thin southern Laurentide ice sheet recorded by Mississippi drainage. Nature, 502(7473), pp.668-671.

Willard, D.A., Bernhardt, C.E., Weimer, L., Cooper, S.R., Gamez, D. and Jensen, J., 2004. Atlas of pollen and spores of the Florida Everglades. *Palynology*, *28*(1), pp.175-227.

Williams, J.W., Grimm, E.G., Blois, J., Charles, D.F., Davis, E., Goring, S.J., Graham, R., Smith, A.J., Anderson, M., Arroyo-Cabrales, J., Ashworth, A.C., Betancourt, J.L., Bills, B.W., Booth, R.K., Buckland, P., Curry, B., Giesecke, T., Hausmann, S., Jackson, S.T., Latorre, C., Nichols, J., Purdum, T., Roth, R.E., Stryker, M., Takahara, H., (2018). The Neotoma Paleoecology Database: A multi-proxy, international community-curated data resource. Quaternary Research 89, 156-177.

Zhang, J., Yu, H., Jia, G., Chen, F. and Liu, Z., 2010. Terrestrial n-alkane signatures in the middle Okinawa Trough during the post-glacial transgression: control by sea level and paleovegetation confounded by offshore transport. Geo-Marine Letters, 30(2), pp.143-150.

Zonneveld, K.A.F., Marret, F., Versteegh, G.J.M., Bogus, K., Bonnet, S., Bouimetarhan, I., Crouch, E., De Vernal, A., Elshanawany, R., Edwards, L. and Esper, O., (2013). Geographic distribution of dinoflagellate cysts in surface sediments. Pangaea.

Zonneveld, K.A.F. and Pospelova V. (2015). A determination key for modern dinoflagellate cysts. Palynology 39 (3), 387- 409.

9. Appendix

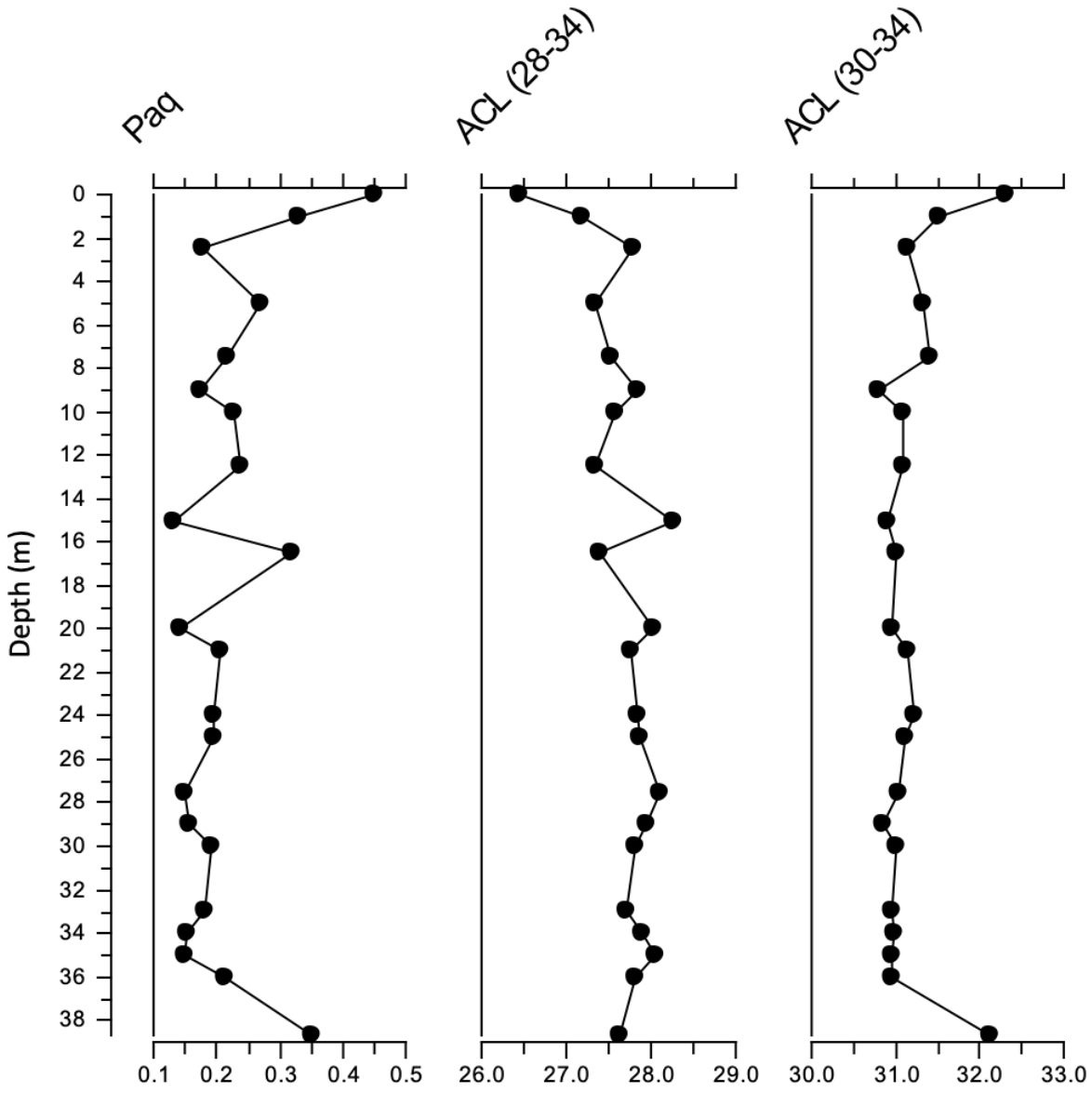

Appendix 1. *P_{aq}, and ACL of Fatty Acid extraction results*